

1

2

3

4

5

(CDF Collaboration)

PRD Draft v1.0

September 1, 2006

6

Abstract

7

8

9

10

11

12

13

14

15

16

We report on new measurements of the inclusive jet production cross section as a function of the jet transverse momentum in $p\bar{p}$ collisions at $\sqrt{s} = 1.96$ TeV using data collected with the upgraded Collider Detector at Fermilab in Run II, corresponding to an integrated luminosity of 1.0 fb^{-1} . The measurements are carried out in five different jet rapidity regions for jets with $|y^{\text{jet}}| < 2.1$ and transverse momentum in the range $54 < p_{\text{T}}^{\text{jet}} < 700$ GeV/c. Next-to-leading order perturbative QCD predictions are in good agreement with the measured cross sections after the necessary non-perturbative parton-to-hadron corrections are included.

Measurement of the Inclusive Jet Cross Section using the k_T algorithm in $p\bar{p}$ Collisions at $\sqrt{s} = 1.96$ TeV

September 1, 2006

1 Introduction

The measurement of the inclusive jet cross section as a function of the jet transverse momentum, p_T^{jet} , in $p\bar{p}$ collisions at $\sqrt{s} = 1.96$ TeV constitutes a test of perturbative QCD (pQCD) [1] predictions over more than eight orders of magnitude in cross section and probes distances down to 10^{-19} m. The increased center-of-mass energy and integrated luminosity in Run II at the Tevatron have allowed to measure the jet cross section for jets with transverse momentum up to about 700 GeV/c [2, 3], thus extending the p_T^{jet} range by more than 150 GeV/c compared to Run I [4, 5]. In particular, the CDF experiment recently published results [2] on inclusive jet production using the k_T algorithm [6, 7] for jets with $p_T^{\text{jet}} > 54$ GeV/c and rapidity [8] in the region $0.1 < |y^{\text{jet}}| < 0.7$, which are well described by NLO pQCD predictions [9]. The pQCD calculations are written as matrix elements, describing the hard interaction between partons, convoluted with parton density functions (PDFs) [10, 11] in the proton and antiproton that require input from the experiments. Inclusive jet cross section measurements from Run I at the Tevatron [5], performed in different jet rapidity regions, have been used to partially constrain the gluon distribution in the proton. As noted in [2], the pQCD predictions are affected by the still limited knowledge on the gluon PDF, which translates into a big uncertainty on the theoretical cross sections at high p_T^{jet} . This article presents new measurements of the inclusive jet production cross section as a function of p_T^{jet} in five different jet rapidity regions

1 up to $|y^{\text{jet}}| = 2.1$, using the k_T algorithm and based on 1.0 fb^{-1} of CDF Run
2 II data. The measurements are corrected to the hadron level [12] and com-
3 pared to NLO pQCD predictions. In the forward region, the uncertainties
4 on the measured cross sections, compared to those on the theoretical predic-
5 tions, indicate that the measurements reported in the article will contribute
6 to a better understanding of the gluon PDF inside the proton.

7 2 Experimental setup

8 The CDF II detector (see Figure 1) is described in detail in [13]. Here, the
9 sub-detectors most relevant for this analysis are briefly discussed. The de-
10 tector has a charged particle tracking system immersed in a 1.4 T magnetic
11 field, aligned coaxially with the beam line. A silicon microstrip detector [14]
12 provides tracking over the radial range 1.35 to 28 cm and covers the pseu-
13 dorapidity range $|\eta| \leq 2$. A 3.1 m long open-cell drift chamber, the Central
14 Outer Tracker (COT) [15], covers the radial range from 44 to 132 cm and
15 provides tracking coverage for $|\eta| \leq 1$. Segmented sampling calorimeters,
16 arranged in a projective tower geometry, surround the tracking system and
17 measure the energy flow of interacting particles in $|\eta| \leq 3.6$. The CDF
18 central barrel calorimeter [16] is unchanged from Run I and covers the re-
19 gion $|\eta| < 1$. It consists of an electromagnetic calorimeter (CEM) and an
20 hadronic calorimeter (CHA) segmented into 480 towers of size 0.1 in η and
21 15° in ϕ . The end-wall hadronic calorimeter (WHA) [17] complements the
22 coverage of the central barrel calorimeter in the region $0.6 < |\eta| < 1.0$ and
23 provides additional forward coverage out to $|\eta| < 1.3$. In Run II, new forward
24 scintillator-plate calorimeters [18] replaced the original Run I gas calorime-
25 ter system. The new plug electromagnetic calorimeter (PEM) covers the
26 region $1.1 < |\eta| < 3.6$ while the new hadronic calorimeter (PHA) provides
27 coverage in the $1.3 < |\eta| < 3.6$ region. The calorimetry has a crack at
28 $|\eta| = 0$ (between the two halves of the central barrel calorimeter) and two
29 cracks centered at $|\eta| \sim 1.1$ (in the region between the WHA and the plug
30 calorimeters). The measured energy resolutions for electrons in the elec-
31 tromagnetic calorimeters are $14\%/\sqrt{E_T}$ (CEM) and $16\%/\sqrt{E} \oplus 1\%$ (PEM)
32 where the energies are expressed in GeV. The single-pion energy resolutions
33 in the hadronic calorimeters, as determined in test-beam data, are $75\%/\sqrt{E_T}$
34 (CHA), $80\%/\sqrt{E}$ (WHA) and $80\%/\sqrt{E} \oplus 5\%$ (PHA). Cherenkov counters
35 located in the $3.7 < |\eta| < 4.7$ region [19] measure the average number of

1 inelastic $p\bar{p}$ collisions per bunch crossing and thereby determine the beam
2 luminosity.

3 **3 Jet reconstruction**

The k_T algorithm is used to reconstruct jets in data and Monte Carlo simulated events (see Section VI) from the energy depositions in the calorimeter towers with transverse momentum above 0.1 GeV/c. First, all towers are considered as protojets. The quantities

$$k_{T,i} = p_{T,i}^2 \quad ; \quad k_{T,(i,j)} = \min(p_{T,i}^2, p_{T,j}^2) \cdot \Delta R_{i,j}^2 / D^2, \quad (1)$$

4 are computed for each protojet and pair of protojets respectively, where $p_{T,i}$
5 denotes the transverse momentum of the i^{th} protojet, $\Delta R_{i,j}$ is the distance
6 ($y - \phi$ space) between each pair of protojets, and D is a parameter that
7 approximately controls the size of the jet. All $k_{T,i}$ and $k_{T,(i,j)}$ values are then
8 collected into a single sorted list. In this combined sorted list, if the smallest
9 quantity is of the type $k_{T,i}$, the corresponding protojet is promoted to be a jet
10 and removed from the list. Otherwise, if the smallest quantity is of the type
11 $k_{T,(i,j)}$, the protojets are combined into a single protojet by summing up their
12 four-vector components. The procedure is iterated over protojets until the
13 list is empty. The jet transverse momentum, rapidity, and azimuthal angle
14 are denoted as $p_{T,CAL}^{\text{jet}}$, y_{CAL}^{jet} , and ϕ_{CAL}^{jet} , respectively. The same jet algorithm
15 is applied to the final-state particles in the Monte Carlo event samples to
16 search for jets at the hadron level. In this case, no cut on the minimum
17 transverse momentum of the particles is applied. The resulting hadron-level
18 jet variables are denoted as $p_{T,HAD}^{\text{jet}}$, y_{HAD}^{jet} , and ϕ_{HAD}^{jet} .

19 **4 Event selection**

20 The measurements presented in this article correspond to a total integrated
21 luminosity of $0.99 \pm 0.06 \text{ fb}^{-1}$ of data collected by the CDF experiment
22 in Run II. Events were selected *online* using three-level trigger paths [20],
23 based on the measured energy deposits in the calorimeter towers, with dif-
24 ferent thresholds on the jet transverse energies and different prescales (see
25 Table I). In the first-level trigger, a single trigger tower with transverse en-
26 ergy above 5 GeV or 10 GeV, depending on the trigger path, is required. In

1 the second-level trigger, calorimeter clusters are formed around the selected
 2 trigger towers. The events are required to have at least one second-level
 3 trigger cluster with transverse energy above a given threshold, which varies
 4 between 15 and 90 GeV for the different trigger paths. In the third-level
 5 trigger, jets are reconstructed using the CDF Run I cone algorithm [21] and
 6 the events are required to have at least one jet with transverse energy above
 7 20 to 100 GeV depending on the trigger path.

Trigger Path	Level 1 tower E_T [GeV]	Level 2 cluster E_T [GeV]	Level 3 jet E_T [GeV]	eff. prescale
Jet 20	5	15	20	775
Jet 50	5	40	50	34
Jet 70	10	60	70	8
Jet 100	10	90	100	1

Table 1: Summary of trigger paths, trigger thresholds and effective prescales employed to collect the data.

8 Jets are then searched for using the k_T algorithm, as explained above, with
 9 $D = 0.7$. For each trigger data sample, the threshold on the minimum $p_{T,CAL}^{jet}$,
 10 in each $|y_{CAL}^{jet}|$ region, is chosen in such a way that the trigger selection is
 11 fully efficient and the corresponding prescale is taken into account. As an
 12 example, Figure 2 shows, for jets in the region $0.1 < |y_{CAL}^{jet}| < 0.7$, the trigger
 13 efficiency curves as a function of $p_{T,CAL}^{jet}$ for the different trigger data samples.
 14 The following selection criteria have been imposed:

- 15 • The events are selected to have at least one reconstructed primary
 16 vertex with z -position within 60 cm around the nominal interaction
 17 point.
- 18 • Events are required to have at least one jet with rapidity in the region
 19 $|y_{CAL}^{jet}| < 2.1$ and corrected transverse momentum (see below) above
 20 54 GeV/c, which constitutes the minimum jet transverse momentum
 21 considered in the analysis. The measurements are limited to jets with
 22 $|y_{CAL}^{jet}| < 2.1$ to avoid contributions from the proton/antiproton rem-
 23nants that would affect the measured $p_{T,CAL}^{jet}$ in the most forward region
 24 of the calorimeter.
- 25 • In order to remove beam-related backgrounds and cosmic rays, the
 26 events are required to fulfill $\cancel{E}_T/\sqrt{\Sigma E_T} < F(p_{T,CAL}^{leading\ jet})$, where \cancel{E}_T de-

1 notes the missing transverse energy [22] and $\Sigma E_T = \sum_i E_T^i$ is the total
 2 transverse energy of the event, as measured using calorimeter towers
 3 with E_T^i above 0.1 GeV. The threshold function $F(p_{T,CAL}^{\text{leading jet}})$ is defined
 4 as $F(p_T^{\text{jet}}) = \min(2 + 0.0125 \times p_T^{\text{jet}}, 7)$, where $p_{T,CAL}^{\text{leading jet}}$ is the uncorrected
 5 transverse momentum of the leading jet (highest p_T^{jet}) and the units are
 6 GeV. This criterion is designed to preserve more than 95% of the QCD
 7 events, as determined from Monte Carlo studies. A visual scan for
 8 $p_{T,CAL}^{\text{jet}} > 400$ GeV/c showed no remaining backgrounds.

9 Measurements are carried out in five different y_{CAL}^{jet} regions: $|y_{CAL}^{\text{jet}}| < 0.1$,
 10 $0.1 < |y_{CAL}^{\text{jet}}| < 0.7$, $0.7 < |y_{CAL}^{\text{jet}}| < 1.1$, $1.1 < |y_{CAL}^{\text{jet}}| < 1.6$, and $1.6 <$
 11 $|y_{CAL}^{\text{jet}}| < 2.1$, where the different boundaries are dictated by the layout of the
 12 CDF calorimeter system.

13 5 Effect of multiple $p\bar{p}$ interactions

14 The measured jet transverse momentum includes additional contributions
 15 from multiple proton-antiproton interactions per bunch crossing at high in-
 16 stantaneous luminosity. The data used in this measurement were collected at
 17 Tevatron instantaneous luminosities between $0.2 \times 10^{31} \text{cm}^{-2} \text{s}^{-1}$ and $16.3 \times$
 18 $10^{31} \text{cm}^{-2} \text{s}^{-1}$ with an average of $4.1 \times 10^{31} \text{cm}^{-2} \text{s}^{-1}$, for which, in average, 1.5
 19 inelastic proton-antiproton interactions per bunch crossing are expected. At
 20 the highest instantaneous luminosities considered, an average of 5.9 inter-
 21 actions per bunch crossing are produced. This mainly affects the measured
 22 cross section at low p_T^{jet} where the contributions are sizeable. In CDF, multi-
 23 ple interactions are identified via the presence of additional primary vertices
 24 reconstructed from charged particles. The measured jet transverse momenta
 25 are corrected for this effect by removing a certain amount of transverse mo-
 26 mentum, $\delta_{p_T}^{\text{MI}}$, for each additional primary vertex, as determined from the
 27 data by requiring that, after the correction is applied, the ratio of cross
 28 sections at low and high instantaneous luminosities does not show any p_T^{jet}
 29 dependence. The study is carried out separately in each y_{CAL}^{jet} region, and the
 30 results are consistent with a common value $\delta_{p_T}^{\text{MI}} = 1.86 \pm 0.23$ GeV/c across
 31 the whole rapidity range.

6 Monte Carlo simulation

Monte Carlo event samples are used to determine the response of the detector and the correction factors to the hadron level. The generated samples are passed through a full CDF detector simulation (based on GEANT3 [23] where the GFLASH [24] package is used to simulate the energy deposition in the calorimeters) and then reconstructed and analyzed using the same analysis chain as in the data. Samples of simulated inclusive jet events have been generated using PYTHIA 6.203 [25] and HERWIG 6.4 [26] Monte Carlo generators. CTEQ5L [27] parton distribution functions are used for the proton and antiproton. The PYTHIA samples have been created using a special tuned set of parameters, denoted as PYTHIA-TUNE A [28], that includes enhanced contributions from initial-state gluon radiation and secondary parton interactions between remnants. Tune A was determined as a result of dedicated studies of the underlying event using the CDF Run I data [29] and has been shown to properly describe the measured jet shapes in Run II [30]. In the case of PYTHIA, fragmentation into hadrons is carried out using the string model [31] as implemented in JETSET [32], while HERWIG implements the cluster model [33].

7 Simulation of the calorimeter response to jets

Dedicated studies have been performed to validate the Monte Carlo description of the calorimeter response to jets in the data for the different $|y_{\text{CAL}}^{\text{jet}}|$ regions. Previous results [2] for jets with $0.1 < |y_{\text{CAL}}^{\text{jet}}| < 0.7$ indicate that the simulation properly reproduces both the average jet momentum and the jet momentum resolution as measured in the data. The study is performed for the rest of $|y_{\text{CAL}}^{\text{jet}}|$ regions using jets in $0.1 < |y_{\text{CAL}}^{\text{jet}}| < 0.7$ as reference. An exclusive dijet sample is selected, in data and Monte Carlo events, with the following criteria:

- Events are selected to have one and only one reconstructed primary vertex with z -position within 60 cm around the nominal interaction point.
- Events are required to have exactly two jets with $p_{\text{T,CAL}}^{\text{jet}} > 10 \text{ GeV}/c$,

1 where one of the jets must be in the region $0.1 < |y_{\text{CAL}}^{\text{jet}}| < 0.7$.

2 • $E_T/\sqrt{\Sigma E_T} < F(p_{\text{T,CAL}}^{\text{leading jet}})$, as explained above.

3 First, the bisector method [34] is applied to data and Monte Carlo exclusive
 4 dijet events to test the accuracy of the simulated jet momentum resolution in
 5 the detector. Figure 3 shows the ratio between the jet momentum resolution
 6 in data and Monte Carlo events, $\sigma_{\text{D}}^{\text{DATA}}/\sigma_{\text{D}}^{\text{MC}}$, as determined by the bisector
 7 method, in different $|y_{\text{CAL}}^{\text{jet}}|$ regions as a function of the average $p_{\text{T,CAL}}^{\text{jet}}$ of the
 8 dijet event. The study indicates that the Monte Carlo simulation systemati-
 9 cally underestimates the measured jet momentum resolution by 6 % and 10 %
 10 for jets in the regions $0.7 < |y_{\text{CAL}}^{\text{jet}}| < 1.1$ and $1.6 < |y_{\text{CAL}}^{\text{jet}}| < 2.1$, respectively,
 11 and with no significant $p_{\text{T,CAL}}^{\text{jet}}$ dependence. An additional smearing of the
 12 reconstructed jet transverse momenta is applied to the Monte Carlo events
 13 to account for this effect. In the region $1.1 < |y_{\text{CAL}}^{\text{jet}}| < 1.6$, the measured jet
 14 momentum resolution is overestimated by 5% in the simulation. The effect on
 15 the final result is included via slightly modified unfolding factors (see below).
 16 For jets with $|y_{\text{CAL}}^{\text{jet}}| < 0.1$, the Monte Carlo simulation properly describes
 17 the measured jet momentum resolution. After corrections have been applied
 18 to the Monte Carlo events, data and simulation agree. A rather conservative
 19 *relative* $\pm 8\%$ variation (see Figure 3) over the whole range in $p_{\text{T,CAL}}^{\text{jet}}$ and
 20 $|y_{\text{CAL}}^{\text{jet}}|$ is considered in the study of systematic uncertainties.

The average jet momentum calorimeter response in the simulation is then
 tested comparing the $p_{\text{T,CAL}}^{\text{jet}}$ balance in data and Monte Carlo exclusive dijet
 events. The variable β , defined as¹

$$\beta = \frac{1 + \langle \Delta \rangle}{1 - \langle \Delta \rangle}, \quad \text{with} \quad \Delta = \frac{p_{\text{T,CAL}}^{\text{tested jet}} - p_{\text{T,CAL}}^{\text{ref. jet}}}{p_{\text{T,CAL}}^{\text{tested jet}} + p_{\text{T,CAL}}^{\text{ref. jet}}}, \quad (2)$$

21 is computed in data and simulated events in bins of $(p_{\text{T,CAL}}^{\text{tested jet}} + p_{\text{T,CAL}}^{\text{ref. jet}})/2$,
 22 where $p_{\text{T,CAL}}^{\text{ref. jet}}$ denotes the transverse momentum of the jet in the region $0.1 <$
 23 $|y_{\text{CAL}}^{\text{jet}}| < 0.7$, and $p_{\text{T,CAL}}^{\text{tested jet}}$ is the transverse momentum of the jet in the $|y_{\text{CAL}}^{\text{jet}}|$
 24 region under study. Figure 4 presents the ratios $\beta_{\text{DATA}}/\beta_{\text{MC}}$ as a function
 25 of $p_{\text{T,CAL}}^{\text{jet}} = p_{\text{T,CAL}}^{\text{tested jet}}$ in the different $|y_{\text{CAL}}^{\text{jet}}|$ bins. The study indicates that
 26 small corrections are required around calorimeter cracks, $|y_{\text{CAL}}^{\text{jet}}| < 0.1$ and

¹If considered event-by-event, β is equivalent to $p_{\text{T,CAL}}^{\text{tested jet}}/p_{\text{T,CAL}}^{\text{ref. jet}}$. However, Equation 2
 is preferred since Δ follows a gaussian distribution while the ratio $p_{\text{T,CAL}}^{\text{tested jet}}/p_{\text{T,CAL}}^{\text{ref. jet}}$ suffers
 from important non-gaussian tails.

1 $1.1 < |y_{\text{CAL}}^{\text{jet}}| < 1.6$, as well as in the most forward region, $1.6 < |y_{\text{CAL}}^{\text{jet}}| < 2.1$.
 2 For jets with $|y_{\text{CAL}}^{\text{jet}}| > 1.1$, the correction shows a non-linear $p_{\text{T,CAL}}^{\text{jet}}$ depen-
 3 dence, and at very high $p_{\text{T,CAL}}^{\text{jet}}$ several parameterizations are considered. The
 4 difference observed in the final results, using different parameterizations, is
 5 included as part of the total systematic uncertainty.

6 8 Reconstruction of the jet variables

7 The reconstruction of the jet variables in the detector is studied using Monte
 8 Carlo event samples, with modified jet energy response in the calorimeter as
 9 described in the previous section, and matched pair of jets, in $(\eta - \phi)$ space,
 10 at the calorimeter and hadron levels. These studies indicate that the angular
 11 variables of a jet are reconstructed with no significant systematic shift and
 12 with a resolution better than 0.05 units in y and ϕ at low $p_{\text{T,CAL}}^{\text{jet}}$, improving
 13 as $p_{\text{T,CAL}}^{\text{jet}}$ increases. The measured jet transverse momentum systematically
 14 underestimates that of the hadron level jet. This is mainly attributed to
 15 the non-compensating nature of the calorimeter [35]. For jets with $p_{\text{T,CAL}}^{\text{jet}}$
 16 about 50 GeV/c, the jet transverse momentum is reconstructed with an aver-
 17 age shift that varies between -9% and -30% , depending on the jet rapidity
 18 region, and a resolution between 10% and 16%. The jet reconstruction im-
 19 proves as $p_{\text{T,CAL}}^{\text{jet}}$ increases. For jets with $p_{\text{T,CAL}}^{\text{jet}}$ about 500 GeV/c, the average
 20 shift is -7% and the resolution is about 7%.

21 9 Unfolding

22 The measured $p_{\text{T,CAL}}^{\text{jet}}$ distributions in the different $|y_{\text{CAL}}^{\text{jet}}|$ regions are unfolded
 23 back to the hadron level using Monte Carlo event samples. PYTHIA-TUNE A
 24 provides a reasonable description of the different jet and underlying event
 25 quantities, and is used to determine the correction factors in the unfolding
 26 procedure. In order to avoid any potential bias on the correction factors due
 27 to the particular PDF set used during the generation of the Monte Carlo
 28 samples, which translates into slightly different simulated $p_{\text{T,CAL}}^{\text{jet}}$ distribu-
 29 tions, the underlying \hat{p}_t spectra in PYTHIA-TUNE A is re-weighted until the
 30 Monte Carlo samples accurately follow each of the measured $p_{\text{T,CAL}}^{\text{jet}}$ distri-
 31 butions. The unfolding is carried out in two steps.

First, an average correction is computed separately in each jet rapidity

region using matched pairs of jets at the calorimeter and hadron levels. The correlation $\langle p_{T,HAD}^{jet} - p_{T,CAL}^{jet} \rangle$ vs $\langle p_{T,CAL}^{jet} \rangle$ (see Figure 5), computed in bins of $(p_{T,HAD}^{jet} + p_{T,CAL}^{jet})/2$, is used to extract correction factors which are then applied to the measured jets to obtain the corrected transverse momenta, $p_{T,COR}^{jet}$. In each jet rapidity region, a raw cross section is defined as

$$\frac{d^2\sigma}{dp_{T,COR}^{jet} dy_{CAL}^{jet}} = \frac{1}{\mathcal{L}} \frac{N_{COR}^{jet}}{\Delta p_{T,COR}^{jet} \Delta y_{CAL}^{jet}}, \quad (3)$$

1 where N_{COR}^{jet} denotes the number of jets in a given $p_{T,COR}^{jet}$ bin, $\Delta p_{T,COR}^{jet}$ is
 2 the size of the bin, Δy_{CAL}^{jet} denotes the size of the considered region in y_{CAL}^{jet} ,
 3 and \mathcal{L} is the luminosity.

Second, each measurement is corrected for acceptance and smearing effects using a bin-by-bin unfolding procedure, which also accounts for the efficiency of the selection criteria. The unfolding factors, defined as

$$U(p_{T,COR}^{jet}, y_{CAL}^{jet}) = \frac{d^2\sigma/dp_{T,HAD}^{jet} dy_{HAD}^{jet}}{d^2\sigma/dp_{T,COR}^{jet} dy_{CAL}^{jet}}, \quad (4)$$

4 are extracted from Monte Carlo event samples and applied to the measured
 5 $p_{T,COR}^{jet}$ distributions to obtain the final results. As shown in Figure 6, the
 6 factor $U(p_{T,COR}^{jet}, y_{CAL}^{jet})$ increases with $p_{T,COR}^{jet}$ and presents a moderate y_{CAL}^{jet} -
 7 bin dependence. At very low $p_{T,COR}^{jet}$, the unfolding factor varies between
 8 1.02 and 1.06 for different rapidity regions. For jets with $p_{T,COR}^{jet}$ about 300
 9 GeV/c, the factor varies between 1.1 and 1.2, and increases up to 1.3 - 1.4
 10 at very high $p_{T,COR}^{jet}$. In the region $1.1 < |y_{CAL}^{jet}| < 1.6$, the unfolding factor
 11 includes an additional correction, $f_U(p_{T,COR}^{jet})$, to account for the fact that
 12 the Monte Carlo simulation overestimates the jet momentum resolution in
 13 that region (see section VII). The factor $f_U(p_{T,COR}^{jet})$ is computed from Monte
 14 Carlo samples as the ratio of the nominal $p_{T,HAD}^{jet}$ distribution smeared using
 15 the measured and simulated jet momentum resolution, as determined by the
 16 bisector method. The factor $f_U(p_{T,COR}^{jet})$ is about 1.03 and shows no significant
 17 $p_{T,COR}^{jet}$ dependence.

18 **10 Systematic uncertainties**

19 A detailed study of the systematic uncertainties on the measurements was
 20 carried out [36]. Tables II-III collect the different contributions to the total

1 systematic uncertainty in each p_T^{jet} bin and $|y^{\text{jet}}|$ region:

- 2 • The measured jet energies were varied by $\pm 2\%$ at low p_T^{jet} to $\pm 2.7\%$ at
3 high p_T^{jet} to account for the uncertainty on the absolute energy scale in
4 the calorimeter [37]. This introduces an uncertainty on the measured
5 cross sections which varies between $\pm 9\%$ at low p_T^{jet} and $^{+61\%}_{-39\%}$ at high
6 p_T^{jet} , and dominates the total systematic uncertainty on the different
7 measurements.
- 8 • Several sources of systematic uncertainty on the ratio $\beta_{\text{DATA}}/\beta_{\text{MC}}$ were
9 considered for the different $|y^{\text{jet}}|$ regions:
 - 10 – The uncertainty on the definition of the exclusive dijet sample in
11 data and Monte Carlo events introduces a $\pm 0.5\%$ uncertainty on
12 the absolute energy scale for jets outside the region $0.1 < |y^{\text{jet}}| <$
13 0.7 , which translates into an uncertainty on the final results be-
14 tween $\pm 2\%$ at low p_T^{jet} and $\pm 10\%$ at very high p_T^{jet} .
 - 15 – The use of different $\beta_{\text{DATA}}/\beta_{\text{MC}}$ parameterizations for jets with
16 $|y^{\text{jet}}| > 1.1$ introduces an uncertainty on the final results between
17 about $\pm 10\%$ and $\pm 23\%$ at very high p_T^{jet} .
 - 18 – In the region $1.1 < |y^{\text{jet}}| < 1.6$, an additional $^{+0\%}_{-3\%}$ uncertainty on
19 the final result, independent of p_T^{jet} , accounts for variations in the
20 $\beta_{\text{DATA}}/\beta_{\text{MC}}$ ratio due to the overestimation of the jet momentum
21 resolution in the Monte Carlo samples.
- 22 • A $\pm 8\%$ uncertainty on the jet momentum resolution introduces an
23 uncertainty on the final results between $\pm 2\%$ at low p_T^{jet} and $\pm 12\%$ at
24 high p_T^{jet} .
- 25 • The unfolding procedure was repeated using HERWIG instead of PYTHIA-
26 TUNE A to account for the uncertainty on the modeling of the parton
27 cascades and the jet fragmentation into hadrons. This translates into
28 an uncertainty on the measured cross sections between $\pm 2\%$ and $\pm 8\%$
29 at low p_T^{jet} .
- 30 • The unfolding procedure was also carried out using unweighted PYTHIA-
31 TUNE A, to estimate the residual dependence on the p_T^{jet} spectra. This
32 introduces an uncertainty of about $\pm 4\%$ to $\pm 7\%$ above $400 \text{ GeV}/c$,
33 which becomes negligible at low p_T^{jet} .

- 1 • The quoted uncertainty on $\delta_{p_T}^{\text{MI}}$ was taken into account. The maximal
- 2 effect on the measured cross sections is about $\pm 2\%$.
- 3 • Other sources of systematic uncertainties related to the selection crite-
- 4 ria are smaller than 1% and considered negligible.

5 Positive and negative deviations with respect to the nominal values in each
6 p_T^{jet} bin are added separately in quadrature. Figure 7 shows the total sys-
7 tematic uncertainty on the final results as a function of p_T^{jet} in the different
8 $|y^{\text{jet}}|$ regions, where an additional 5.8% uncertainty on the total luminosity
9 is not included.

10 11 QCD Predictions

11 The measurements are compared to parton-level NLO pQCD predictions, as
12 computed using JETRAD [9] with CTEQ6.1M PDFs [10] and the renormaliza-
13 tion and factorization scales (μ_R and μ_F) set to $\mu_0 = \max(p_T^{\text{jet}})/2$. Different
14 sources of uncertainty in the theoretical predictions were considered. The
15 main contribution comes from the uncertainty on the PDFs and was com-
16 puted using the Hessian method [38]. At low p_T^{jet} the uncertainty is about
17 $\pm 5\%$ and approximately independent of y^{jet} . The uncertainty increases as
18 p_T^{jet} and y^{jet} increase. At very high p_T^{jet} , the uncertainty varies between $^{+60\%}$
19 and $^{-40\%}$ for jets with $|y^{\text{jet}}| < 0.1$ and $1.6 < |y^{\text{jet}}| < 2.1$, respectively, and
20 is dominated by the limited knowledge on the gluon PDF. An increase of
21 μ_R and μ_F from μ_0 to $2\mu_0$ changes the theoretical predictions by only few
22 percents. Values significantly smaller than μ_0 lead to unstable NLO results
23 and were not considered.

24 The theoretical predictions include a correction factor, $C_{\text{HAD}}(p_T^{\text{jet}}, y^{\text{jet}})$,
25 that approximately accounts for non-perturbative contributions from the un-
26 derlying event and fragmentation into hadrons (see Figure 8 and Tables IV-
27 V). In each jet rapidity region, C_{HAD} was estimated, using PYTHIA-TUNE A,
28 as the ratio between the nominal $p_{T,\text{HAD}}^{\text{jet}}$ distribution and the one obtained
29 by turning off both the interactions between proton and antiproton remnants
30 and the fragmentation in the Monte Carlo samples. The correction decreases
31 as p_T^{jet} increases and shows a moderate y^{jet} dependence. At low p_T^{jet} , C_{HAD}
32 varies between 1.18 and 1.13 as $|y^{\text{jet}}|$ increases, and it becomes of the or-
33 der of 1.02 at very high p_T^{jet} . The uncertainty on C_{HAD} varies between $\pm 9\%$
34 and $\pm 12\%$ at low p_T^{jet} and decreases down to about $\pm 1\%$ at very high p_T^{jet} ,

1 as determined from the difference between the parton-to-hadron correction
 2 factors obtained using HERWIG instead of PYTHIA-TUNE A.

3 12 Results

4 The measured inclusive jets cross sections, $\frac{d^2\sigma}{dp_T^{\text{jet}} dy^{\text{jet}}}$, refer to hadron level
 5 jets, reconstructed using the k_T algorithm with $D = 0.7$, in the region $p_T^{\text{jet}} >$
 6 $54 \text{ GeV}/c$ and $|y^{\text{jet}}| < 2.1$. Figure 9 shows the measured cross sections as
 7 a function of p_T^{jet} in five different $|y^{\text{jet}}|$ regions compared to NLO pQCD
 8 predictions where, for presentation, each measurement has been scaled by
 9 a given factor. The data are reported in Tables IV-V. The measured cross
 10 sections decrease by more than seven to eight orders of magnitude as p_T^{jet}
 11 increases. Figure 10 shows the ratios data/theory as a function of p_T^{jet} in
 12 the five different $|y^{\text{jet}}|$ regions. Good agreement is observed in the whole
 13 range in p_T^{jet} and y^{jet} between the measured cross sections and the theoretical
 14 predictions. In particular, no significant deviation from the pQCD prediction
 15 is observed for central jets at high p_T^{jet} . χ^2 tests, relative to the nominal pQCD
 16 prediction and performed separately in each $|y^{\text{jet}}|$ region, give probabilities
 17 that vary between 9% and 90%. A global χ^2 test, applied to the all data
 18 points in all $|y^{\text{jet}}|$ regions simultaneously, gives a probability of 7%. In both
 19 cases, a detailed treatment of correlations between systematic uncertainties
 20 was considered, as discussed in appendix A.

21 In addition, Figure 10 shows the ratio of pQCD predictions using MRST2004 [11]
 22 and CTEQ6.1M PDF sets, well inside the theoretical and experimental un-
 23 certainties. In the most forward region, the uncertainty on the measured
 24 cross section at high p_T^{jet} , compare to that on the theoretical prediction, in-
 25 dicates that the data presented in this article will contribute to a better
 26 understanding of the gluon PDF.

27 Finally, in the region $0.1 < |y^{\text{jet}}| < 0.7$, the analysis is repeated using
 28 different values for D in the k_T algorithm: $D = 0.5$ and $D = 1.0$. In both
 29 cases, good agreement is observed between the measured cross sections and
 30 the NLO pQCD predictions in the whole range in p_T^{jet} (see Figure 11 and
 31 Tables VI-VII). The corresponding χ^2 tests give probabilities of 84% and 22%
 32 for $D = 0.5$ and $D = 1.0$, respectively. As D decreases, the measurement is
 33 less sensitive to contributions from multiple proton-antiproton interactions,
 34 and the presence and proper modeling of the underlying event. For $D = 0.5$
 35 ($D = 1.0$), the value for $\delta_{p_T}^{\text{MI}}$ becomes 1.18 ± 0.12 (3.31 ± 0.47) GeV/c , and

1 the parton-to-hadron correction factor applied to the pQCD predictions is
2 $C_{\text{HAD}} = 1.1$ ($C_{\text{HAD}} = 1.4$) at low $p_{\text{T}}^{\text{jet}}$.

3 **13 Summary and conclusions**

4 In summary, we have presented results on inclusive jet production in $p\bar{p}$
5 collisions at $\sqrt{s} = 1.96$ TeV using the k_{T} algorithm, for jets with trans-
6 verse momentum $p_{\text{T}}^{\text{jet}} > 54$ GeV/c and rapidity in the region $|y^{\text{jet}}| < 2.1$,
7 based on 1.0 fb^{-1} of CDF Run II data. The measured cross sections are in
8 agreement with NLO pQCD predictions after the necessary non-perturbative
9 parton-to-hadron corrections are taken into account. In the forward region,
10 the uncertainties on the measured cross sections, compared to those on the
11 theoretical predictions, indicate that the results reported in this article will
12 contribute to a better understanding of the gluon PDF inside the proton.

13 **Acknowledgments**

14 We thank the Fermilab staff and the technical staffs of the participating in-
15 stitutions for their vital contributions. This work was supported by the U.S.
16 Department of Energy and National Science Foundation; the Italian Istituto
17 Nazionale di Fisica Nucleare; the Ministry of Education, Culture, Sports,
18 Science and Technology of Japan; the Natural Sciences and Engineering Re-
19 search Council of Canada; the National Science Council of the Republic of
20 China; the Swiss National Science Foundation; the A.P. Sloan Foundation;
21 the Bundesministerium fuer Bildung und Forschung, Germany; the Korean
22 Science and Engineering Foundation and the Korean Research Foundation;
23 the Particle Physics and Astronomy Research Council and the Royal Society,
24 UK; the Russian Foundation for Basic Research; the Comision Interministe-
25 rial de Ciencia y Tecnologia, Spain; in part by the European Community's
26 Human Potential Programme under contract HPRN-CT-2002-00292; and the
27 Academy of Finland.

28 **References**

- 29 [1] D.J. Gross and F. Wilczek, Phys. Rev. D **8**, 3633 (1973).
30 H.Fritzsch, M. Gell-Mann and H. Leutwyler, Phys. Lett. **B47**, 365

- 1 (1973).
- 2 [2] A. Abulencia *et al.* (CDF Collaboration), Phys. Rev. Lett. **96**, 122001
3 (2006).
- 4 [3] A. Abulencia *et al.*, hep-ex/0512020.
- 5 [4] T. Affolder *et al.* (CDF Collaboration), Phys. Rev. D **64**, 032001 (2001).
6 [Erratum-ibid. D **65**, 039903 (2002)].
- 7 [5] B. Abbott *et al.* (DØ Collaboration), Phys. Rev. Lett. **82**, 2451 (1999).
- 8 [6] S. Catani *et al.*, Nucl. Phys. B **406**, 187 (1993).
- 9 [7] S.D. Ellis and D.E. Soper, Phys. Rev. D **48**, 3160 (1993).
- 10 [8] We use a cylindrical coordinate system about the beam axis in which θ
11 is the polar angle and ϕ is the azimuthal angle. We define $E_T = E \sin\theta$,
12 $p_T = p \sin\theta$, $\eta = -\ln(\tan(\frac{\theta}{2}))$, and $y = \frac{1}{2}\ln(\frac{E+p_z}{E-p_z})$.
- 13 [9] W.T. Giele, E.W.N. Glover and David A. Kosower, Nucl. Phys. B **403**,
14 633 (1993).
- 15 [10] J. Pumplin *et al.*, JHEP **0207**, 012 (2002).
- 16 [11] A. D. Martin *et al.*, Eur. Phys. J. C **23**, 73 (2002).
- 17 [12] The hadron level in the Monte Carlo generators is defined using all
18 final-state particles with lifetime above 10^{-11} s.
- 19 [13] D. Acosta *et al.* (CDF Collaboration), Phys. Rev. D **71**, 032001 (2005).
- 20 [14] A. Sill *et al.*, Nucl. Instrum. Meth. A **447**, 1 (2000).
21 A. Affolder *et al.*, Nucl. Instrum. Meth. A **453**, 84 (2000).
22 C.S. Hill, Nucl. Instrum. Meth. A **530**, 1 (2000).
- 23 [15] T. Affolder *et al.*, Nucl. Instrum. Meth. A **526**, 249 (2004).
- 24 [16] L. Balka *et al.*, Nucl. Instrum. Meth. A **267**, 272 (1988).
- 25 [17] S. Bertolucci *et al.*, Nucl. Instrum. Meth. A **267**, 301 (1988).

- 1 [18] R. Oishi, Nucl. Instr. Meth. A **453**, 277 (2000).
2 M. G. Albrow et al., Nucl. Instr. Meth. A **480**, 524 (2002).
- 3 [19] D. Acosta *et al.*, Nucl. Instrum. Meth., A **494**, 57 (2002).
- 4 [20] B. L. Winer, Int. J. Mod. Phys. A **16S1C**, 1169 (2001).
- 5 [21] CDF Collab., F. Abe et al., Phys. Rev. D **45**, 1448 (1992).
- 6 [22] \cancel{E}_T is defined as the norm of $-\sum_i E_T^i \cdot \vec{n}_i$, where \vec{n}_i is the unit vec-
7 tor in the azimuthal plane that points from the beamline to the i-th
8 calorimeter tower.
- 9 [23] R. Brun *et al.*, Tech. Rep. CERN-DD/EE/84-1, 1987.
- 10 [24] G. Grindhammer, M. Rudowicz and S. Peters, Nucl. Instrum. Meth. A
11 **290**, 469 (1990).
- 12 [25] T. Sjöstrand *et al.*, Comp. Phys. Comm. **135**, 238 (2001).
- 13 [26] G. Corcella *et al.*, JHEP **0101**, 010 (2001).
- 14 [27] H.L. Lai *et al.*, Eur. Phys. J. C **12**, 375 (2000).
- 15 [28] PYTHIA-TUNE A Monte Carlo samples are generated using the follow-
16 ing tuned parameters in PYTHIA: PARP(67) = 4.0, MSTP(82) = 4,
17 PARP(82) = 2.0, PARP(84) = 0.4, PARP(85) = 0.9, PARP(86) =
18 0.95, PARP(89) = 1800.0, PARP(90) = 0.25.
- 19 [29] T. Affolder *et al.* (CDF Collaboration), Phys. Rev. D **65**, 092002 (2002).
- 20 [30] D. Acosta *et al.* (CDF Collaboration), Phys. Rev. D **71**, 112002 (2005).
- 21 [31] B. Andersson *et al.*, Phys. Rep. **97**, 31 (1983).
- 22 [32] T. Sjöstrand, Comp. Phys. Comm. **39**, 347 (1986).
- 23 [33] B.R. Webber, Nucl. Phys. B **238**, 492 (1984).
- 24 [34] P. Bagnaia *et al.* (UA2 Collaboration), Phys. Lett. B **144**, 283 (1984).
- 25 [35] S.R. Hahn *et al.*, Nucl. Instrum. Meth. A **267**, 351 (1988).

- 1 [36] Olga Norriella, PhD. Thesis, Universitat Aut3noma de Barcelona, in
2 preparation.
- 3 [37] A. Bhatti *et al.*, hep-ex/0510047.
- 4 [38] J. Pumplin *et al.*, Phys. Rev. D **65**, 014013 (2002).

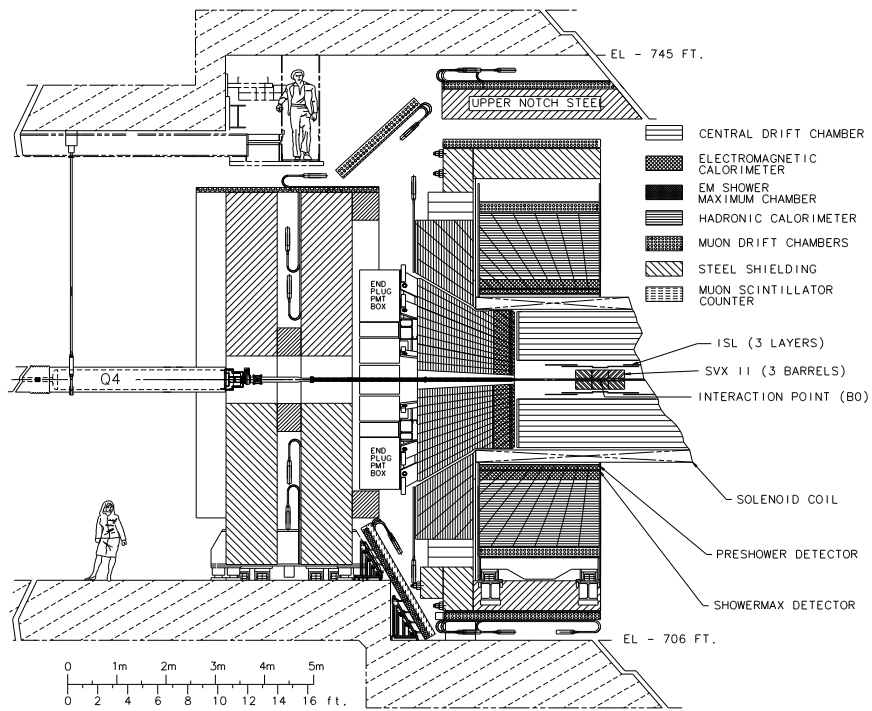


Figure 1: Longitudinal view of half of the CDF II detector.

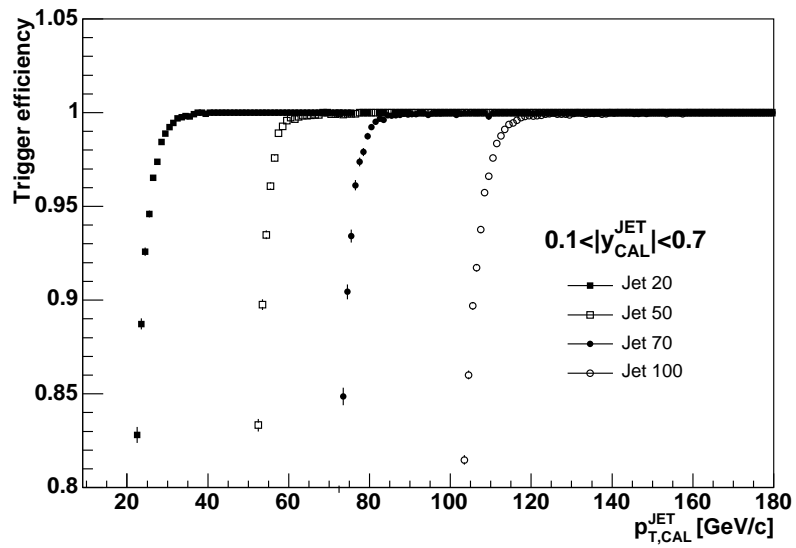


Figure 2: Measured trigger efficiency curves for different trigger datasets as a function of $p_{T,CAL}^{jet}$ in the region $0.1 < |y_{CAL}^{jet}| < 0.7$.

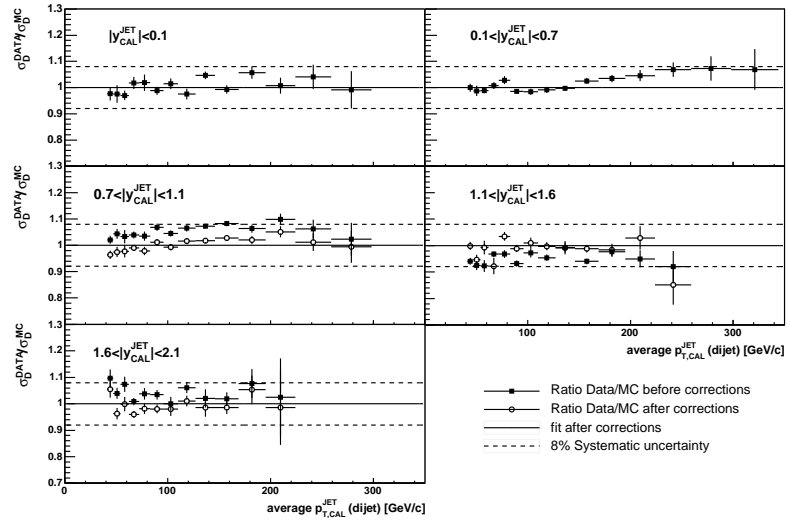


Figure 3: Ratio $\sigma_D^{DATA}/\sigma_D^{MC}$, in different $|y_{CAL}^{jet}|$ regions, as a function of the average $p_{T,CAL}^{jet}$ of the dijet event, before (black dots) and after (open circles) corrections have been applied. The solid lines are fits to the corrected ratios. The dashed lines indicate a $\pm 8\%$ relative variation considered in the study of systematic uncertainties.

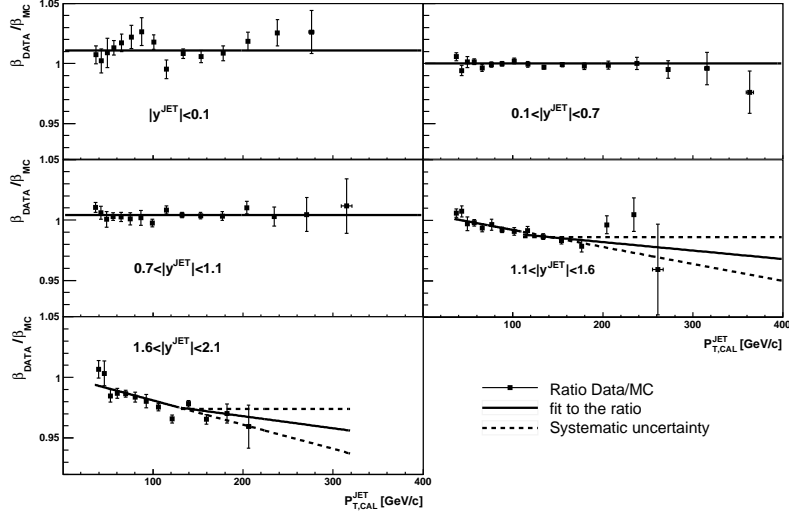


Figure 4: Ratio $\beta_{\text{DATA}}/\beta_{\text{MC}}$ as a function of $p_{\text{T,CAL}}^{\text{jet}}$ in different $|y^{\text{jet}}|$ regions. The solid lines are fits to the ratios. In the region $|y^{\text{jet}}| > 1.1$, the dashed lines indicate different parameterizations used to describe the ratios at high $p_{\text{T,CAL}}^{\text{jet}}$, and are considered in the study of systematic uncertainties.

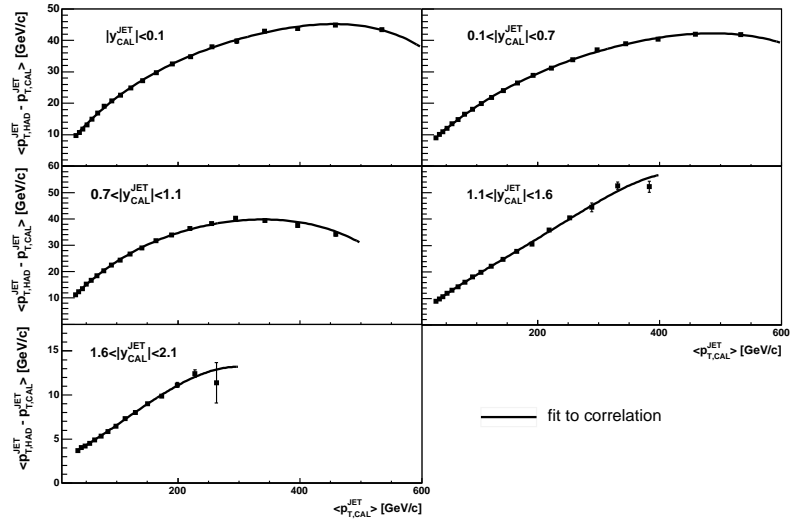


Figure 5: Correlation $\langle p_{T,HAD}^{jet} - p_{T,CAL}^{jet} \rangle$ vs $\langle p_{T,CAL}^{jet} \rangle$, as extracted from PYTHIA TUNE A Monte Carlo events samples, in the different $|y^{jet}|$ regions.

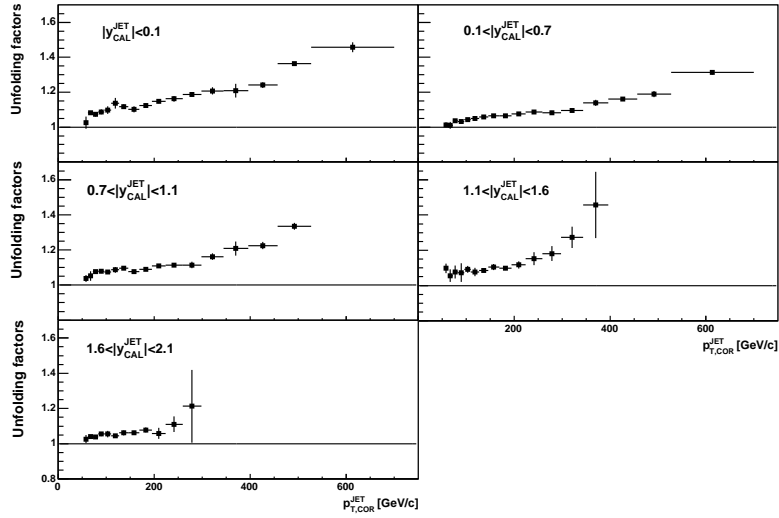


Figure 6: Unfolding factors, $U(p_{T,COR}^{jet}, y_{CAL}^{jet})$, as extracted from PYTHIA TUNE A Monte Carlo events samples, as a function of p_T^{jet} in the different $|y^{jet}|$ regions.

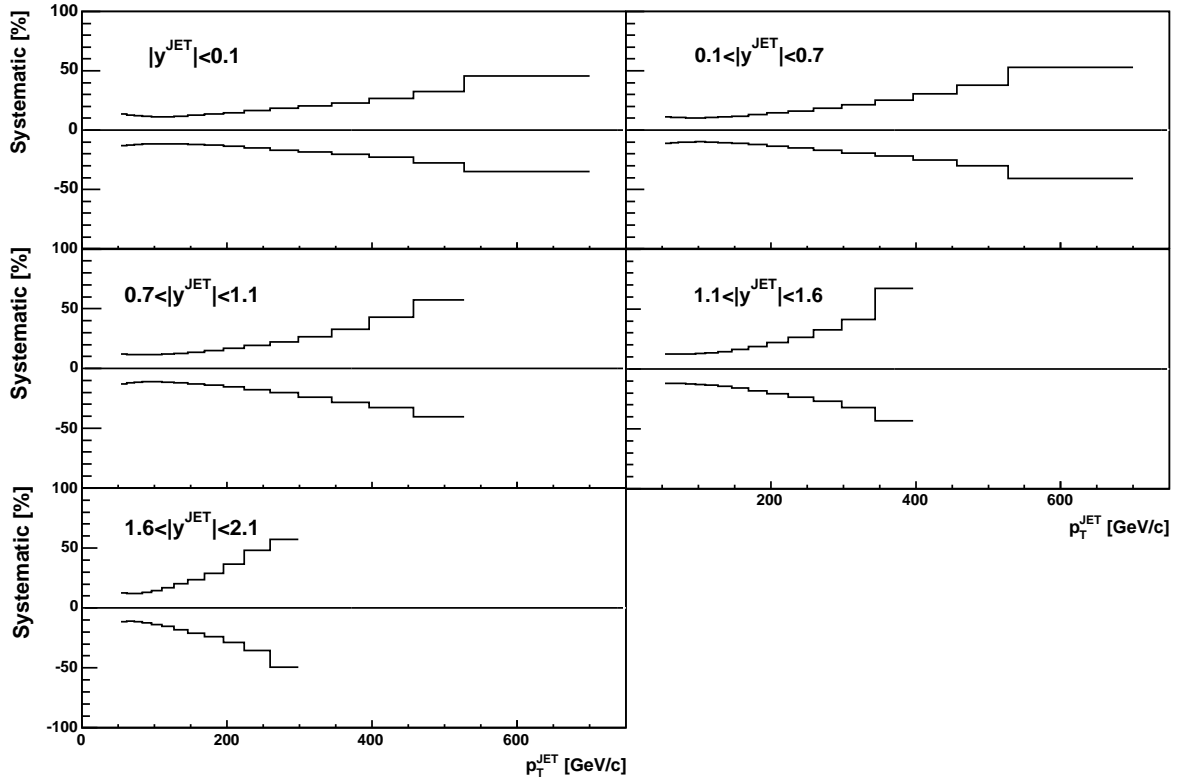


Figure 7: Total systematic uncertainty (in percentage) on the measured inclusive differential jet cross sections as a function p_T^{jet} for the different $|y^{\text{jet}}|$ regions. An additional 5.8% uncertainty on the luminosity is not included.

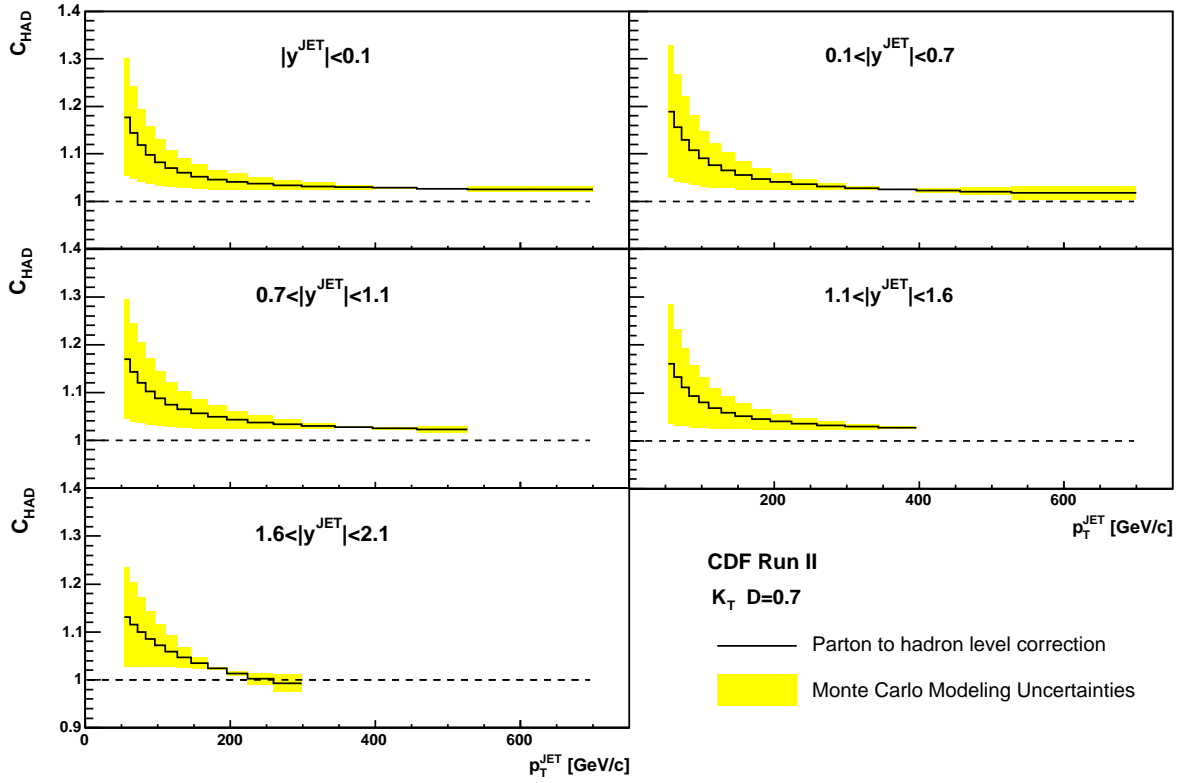


Figure 8: Magnitude of the parton-to-hadron correction, $C_{\text{HAD}}(p_T^{\text{jet}}, y^{\text{jet}})$, used to correct the NLO pQCD predictions. The shaded band indicates the quoted Monte Carlo modeling uncertainty.

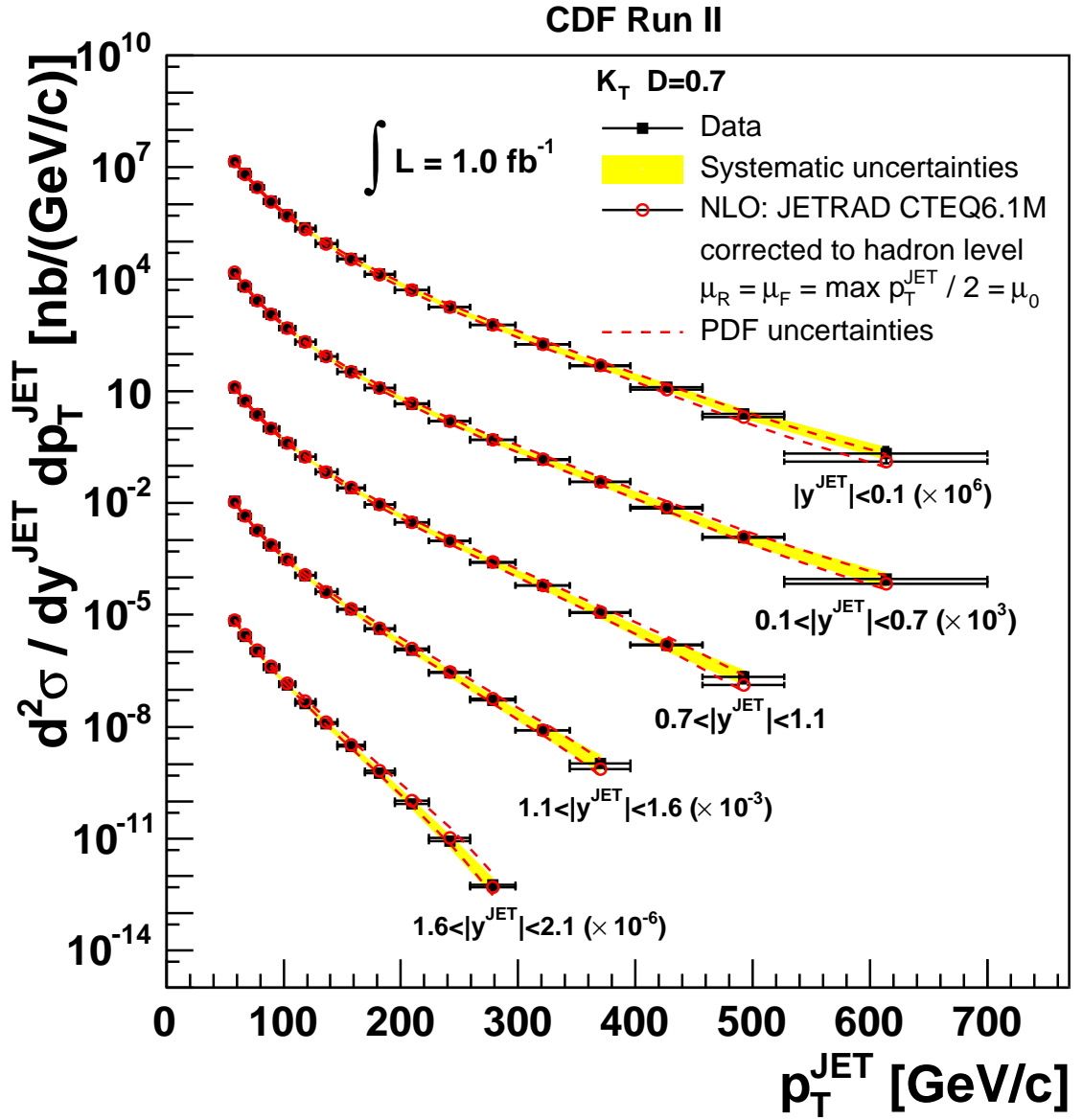


Figure 9: Measured inclusive differential jet cross sections (black dots) as a function of p_T^{jet} for jets with $p_T^{\text{jet}} > 54 \text{ GeV/c}$ in different $|y^{\text{jet}}|$ regions compared to NLO pQCD predictions (open circles). The shaded bands show the total systematic uncertainty on the measurements. A 5.8% uncertainty on the luminosity is not included. The dashed lines indicate the PDF uncertainty on the theoretical predictions. For presentation, each measurement is scaled by a given factor.

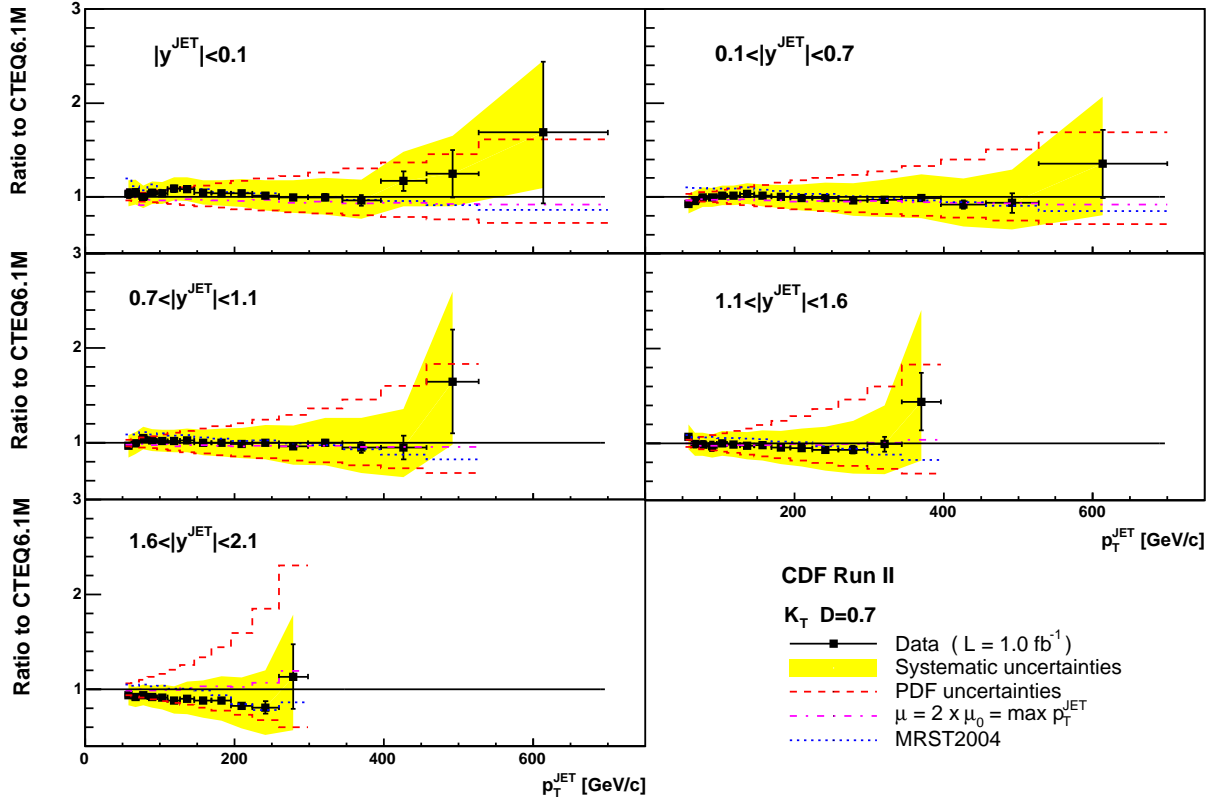


Figure 10: Ratio Data/Theory as a function of p_T^{jet} in different $|y^{\text{jet}}|$ regions. The error bars (shaded bands) show the total statistical (systematic) uncertainty on the data. A 5.8% uncertainty on the luminosity is not included. The dashed lines indicate the PDF uncertainty on the theoretical predictions. The dotted lines present the ratios of MRST2004 and CTEQ6.1M predictions. The dotted-dashed lines show the ratios of predictions with $2\mu_0$ and μ_0 .

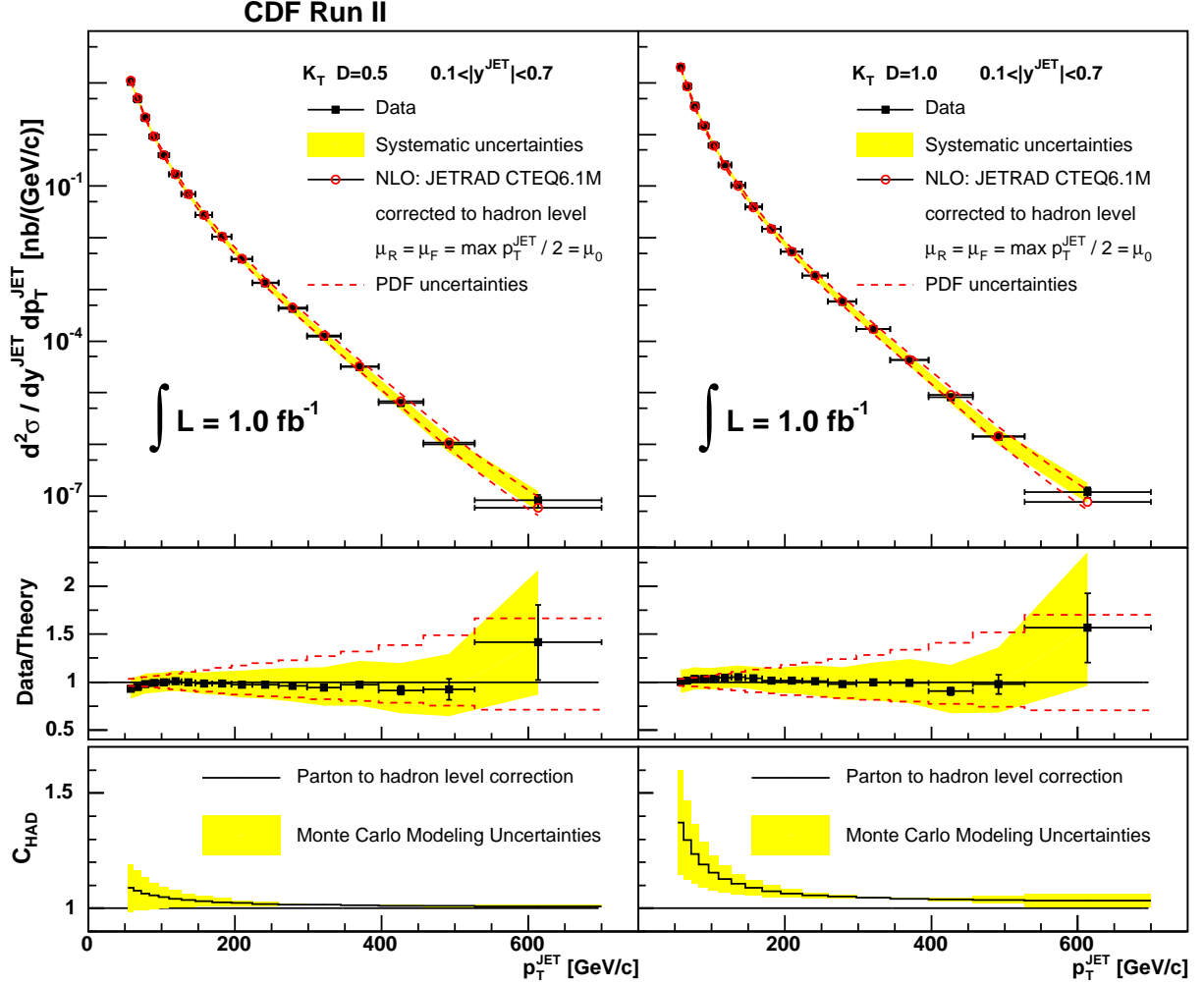


Figure 11: (top) Measured inclusive differential jet cross sections (black dots) as a function of p_T^{jet} for jets with $p_T^{\text{jet}} > 54$ GeV/c and $0.1 < |y^{\text{jet}}| < 0.7$ using $D = 0.5$ (left) and $D = 1.0$ (right), compared to NLO pQCD predictions. The shaded bands show the total systematic uncertainty on the measurements. A 5.8% uncertainty on the luminosity is not included. The dashed lines indicate the PDF uncertainty on the theoretical predictions. (bottom) Magnitude of the parton-to-hadron corrections, $C_{\text{HAD}}(p_T^{\text{jet}})$, used to correct the NLO pQCD predictions for $D = 0.5$ (left) and $D = 1.0$ (right). The shaded bands indicate the quoted Monte Carlo modeling uncertainty.

systematic uncertainties (%) ($ y^{\text{jet}} < 0.1$)								
p_T^{jet} [GeV/c]	jet energy scale	$\beta_{\text{DATA}}/\beta_{\text{MC}}$			resolution	unfolding	p_T^{jet} -spectra	$\delta_{\text{PT}}^{\text{MI}}$
54 - 62	+10.3	+1.4	-	-	+2.8	± 8.2	± 1.5	+1.8
	-9.3	-2.1	-	-	-3.0			-1.7
62 - 72	+9.9	+1.7	-	-	+2.8	± 7.1	± 1.4	+1.6
	-9.4	-2.1	-	-	-3.0			-1.5
72 - 83	+9.6	+1.9	-	-	+2.9	± 6.2	± 1.3	+1.4
	-9.4	-2.1	-	-	-3.0			-1.3
83 - 96	+9.4	+2.1	-	-	+2.9	± 5.4	± 1.1	+1.3
	-9.5	-2.2	-	-	-2.9			-1.1
96 - 110	+9.5	+2.3	-	-	+2.9	± 4.7	± 1.0	+1.1
	-9.6	-2.2	-	-	-2.9			-1.0
110 - 127	+9.8	+2.5	-	-	+3.0	± 4.2	± 0.9	+1.0
	-9.8	-2.3	-	-	-2.9			-0.9
127 - 146	+10.4	+2.7	-	-	+3.1	± 3.7	± 0.8	+0.9
	-10.2	-2.4	-	-	-2.9			-0.8
146 - 169	+11.2	+2.8	-	-	+3.1	± 3.2	± 0.6	+0.8
	-10.8	-2.6	-	-	-3.0			-0.8
169 - 195	+12.4	+2.9	-	-	+3.3	± 2.8	± 0.5	+0.7
	-11.6	-2.7	-	-	-3.0			-0.7
195 - 224	+13.9	+3.0	-	-	+3.4	± 2.5	± 0.4	+0.6
	-12.8	-2.9	-	-	-3.2			-0.7
224 - 259	+15.5	+3.1	-	-	+3.7	± 2.2	± 0.3	+0.6
	-14.3	-3.1	-	-	-3.4			-0.6
259 - 298	+17.4	+3.3	-	-	+4.0	± 2.0	± 0.4	+0.5
	-15.9	-3.4	-	-	-3.6			-0.6
298 - 344	+19.5	+3.6	-	-	+4.3	± 1.8	± 0.6	+0.5
	-17.4	-3.7	-	-	-4.0			-0.6
344 - 396	+22.1	+4.0	-	-	+4.8	± 1.6	± 1.0	+0.4
	-19.1	-4.0	-	-	-4.5			-0.5
396 - 457	+25.7	+4.6	-	-	+5.4	± 1.4	± 1.8	+0.4
	-21.6	-4.4	-	-	-5.1			-0.5
457 - 527	+31.3	+5.3	-	-	+6.1	± 1.3	± 3.1	+0.3
	-26.3	-5.1	-	-	-5.9			-0.5
527 - 700	+43.7	+7.3	-	-	+7.4	± 1.1	± 7.1	+0.3
	-32.9	-6.7	-	-	-7.3			-0.5

systematic uncertainties (%) ($0.1 < y^{\text{jet}} < 0.7$)								
p_T^{jet} [GeV/c]	jet energy scale	$\beta_{\text{DATA}}/\beta_{\text{MC}}$			resolution	unfolding	p_T^{jet} -spectra	$\delta_{\text{PT}}^{\text{MI}}$
54 - 62	+9.5	-	-	-	+2.2	± 5.3	± 0.6	+1.6
	-9.4	-	-	-	-2.5			-1.6
62 - 72	+9.4	-	-	-	+2.1	± 4.7	± 0.6	+1.5
	-9.1	-	-	-	-2.4			-1.4
72 - 83	+9.4	-	-	-	+2.1	± 4.1	± 0.5	+1.3
	-8.9	-	-	-	-2.4			-1.3
83 - 96	+9.4	-	-	-	+2.0	± 3.7	± 0.5	+1.2
	-8.9	-	-	-	-2.3			-1.1
96 - 110	+9.6	-	-	-	+2.0	± 3.3	± 0.5	+1.1
	-9.0	-	-	-	-2.2			-1.0
110 - 127	+10.0	-	-	-	+1.9	± 3.0	± 0.5	+1.0
	-9.3	-	-	-	-2.1			-0.9
127 - 146	+10.6	-	-	-	+1.9	± 2.7	± 0.5	+0.9
	-9.8	-	-	-	-2.1			-0.8
146 - 169	+11.4	-	-	-	+1.9	± 2.4	± 0.4	+0.8
	-10.6	-	-	-	-2.0			-0.8
169 - 195	+12.6	-	-	-	+2.0	± 2.2	± 0.4	+0.7
	-11.7	-	-	-	-2.1			-0.7
195 - 224	+14.1	-	-	-	+2.1	± 2.0	± 0.4	+0.7
	-13.1	-	-	-	-2.1			-0.7
224 - 259	+16.0	-	-	-	+2.2	± 1.8	± 0.3	+0.6
	-14.8	-	-	-	-2.3			-0.6
259 - 298	+18.4	-	-	-	+2.5	± 1.7	± 0.3	+0.6
	-16.7	-	-	-	-2.5			-0.6
298 - 344	+21.3	-	-	-	+2.8	± 1.6	± 0.3	+0.5
	-18.9	-	-	-	-2.9			-0.6
344 - 396	+25.1	-	-	-	+3.4	± 1.5	± 0.5	+0.5
	-21.4	-	-	-	-3.5			-0.5
396 - 457	+30.3	-	-	-	+4.1	± 1.4	± 0.8	+0.4
	-24.7	-	-	-	-4.2			-0.5
457 - 527	+37.7	-	29	-	+5.1	± 1.3	± 1.4	+0.4
	-29.3	-	-	-	-5.2			-0.5
527 - 700	+52.3	-	-	-	+7.3	± 1.2	± 3.6	+0.4
	-39.8	-	-	-	-7.3			-0.5

Table 2: Systematic uncertainties (in percentage) on the measured inclusive jet differential cross section as a function of p_T^{jet} for jets in the regions $|y^{\text{jet}}| < 0.1$ and $0.1 < |y^{\text{jet}}| < 0.7$. An additional 5.8% uncertainty on the luminosity is not included.

systematic uncertainties (%) ($0.7 < |y^{\text{jet}}| < 1.1$)

p_T^{jet} [GeV/c]	jet energy scale	$\beta_{\text{DATA}}/\beta_{\text{MC}}$			resolution	unfolding	p_T^{jet} -spectra	$\delta_{\text{PT}}^{\text{MI}}$
54 - 62	+9.2 -9.9	+2.1 -2.3	—	—	+4.0 -3.8	± 6.3	± 2.0	+1.7 -1.6
62 - 72	+9.2 -9.3	+2.2 -2.3	—	—	+3.8 -3.7	± 5.6	± 1.9	+1.5 -1.4
72 - 83	+9.2 -9.0	+2.3 -2.3	—	—	+3.7 -3.5	± 4.9	± 1.8	+1.3 -1.3
83 - 96	+9.5 -9.0	+2.3 -2.3	—	—	+3.5 -3.4	± 4.4	± 1.8	+1.2 -1.2
96 - 110	+9.9 -9.3	+2.4 -2.4	—	—	+3.4 -3.3	± 3.9	± 1.7	+1.1 -1.1
110 - 127	+10.6 -9.8	+2.5 -2.5	—	—	+3.3 -3.2	± 3.5	± 1.7	+1.0 -1.0
127 - 146	+11.5 -10.7	+2.6 -2.6	—	—	+3.3 -3.1	± 3.2	± 1.7	+0.9 -0.9
146 - 169	+12.6 -11.7	+2.8 -2.7	—	—	+3.3 -3.2	± 2.8	± 1.6	+0.8 -0.8
169 - 195	+14.1 -13.0	+3.0 -2.9	—	—	+3.4 -3.3	± 2.6	± 1.6	+0.8 -0.8
195 - 224	+15.9 -14.6	+3.3 -3.2	—	—	+3.7 -3.5	± 2.3	± 1.7	+0.7 -0.7
224 - 259	+18.1 -16.5	+3.8 -3.6	—	—	+4.1 -3.9	± 2.1	± 1.8	+0.7 -0.7
259 - 298	+21.0 -19.2	+4.4 -4.1	—	—	+4.7 -4.5	± 2.0	± 2.1	+0.6 -0.6
298 - 344	+25.2 -22.7	+5.0 -4.8	—	—	+5.6 -5.3	± 1.8	± 2.4	+0.6 -0.6
344 - 396	+31.5 -26.9	+5.9 -5.6	—	—	+6.8 -6.4	± 1.7	± 3.0	+0.6 -0.6
396 - 457	+41.3 -31.0	+7.2 -6.6	—	—	+8.3 -7.7	± 1.6	± 3.8	+0.5 -0.5
457 - 527	+55.4 -38.3	+10.4 -7.7	—	—	+10.0 -9.1	± 1.5	± 5.0	+0.5 -0.5

systematic uncertainties (%) ($1.1 < |y^{\text{jet}}| < 1.6$)

p_T^{jet} [GeV/c]	jet energy scale	$\beta_{\text{DATA}}/\beta_{\text{MC}}$			resolution	unfolding	p_T^{jet} -spectra	$\delta_{\text{PT}}^{\text{MI}}$
54 - 62	+9.4 -8.6	+2.6 -2.4	—	+0.0 -3.0	+2.9 -3.1	± 6.7	± 1.3	+1.8 -1.8
62 - 72	+9.5 -8.9	+2.5 -2.4	—	+0.0 -3.0	+2.9 -3.0	± 6.4	± 1.1	+1.6 -1.5
72 - 83	+9.8 -9.3	+2.5 -2.5	—	+0.0 -3.0	+2.9 -2.9	± 6.1	± 0.9	+1.4 -1.3
83 - 96	+10.2 -9.8	+2.5 -2.6	—	+0.0 -3.0	+2.9 -2.8	± 5.8	± 0.8	+1.3 -1.2
96 - 110	+10.9 -10.5	+2.6 -2.6	—	+0.0 -3.0	+3.0 -2.9	± 5.6	± 0.6	+1.2 -1.1
110 - 127	+11.7 -11.4	+2.7 -2.8	—	+0.0 -3.0	+3.1 -3.0	± 5.4	± 0.4	+1.1 -1.0
127 - 146	+12.8 -12.6	+2.9 -3.0	—	+0.0 -3.0	+3.4 -3.2	± 5.2	± 0.3	+1.1 -1.0
146 - 169	+14.5 -14.2	+3.3 -3.3	—	+0.0 -3.0	+3.8 -3.6	± 5.0	± 0.1	+1.0 -0.9
169 - 195	+16.9 -16.2	+3.8 -3.7	—	+0.0 -3.0	+4.3 -4.2	± 4.8	± 0.1	+1.0 -0.9
195 - 224	+20.3 -18.6	+4.4 -4.2	+0.7 -0.9	+0.0 -3.0	+5.1 -5.0	± 4.7	± 0.2	+0.9 -0.9
224 - 259	+24.7 -21.2	+5.2 -5.0	+2.6 -2.4	+0.0 -3.0	+6.2 -6.1	± 4.6	± 0.4	+0.9 -0.9
259 - 298	+29.9 -24.1	+6.2 -5.9	+6.3 -4.5	+0.0 -3.0	+7.8 -7.3	± 4.4	± 0.8	+0.9 -0.9
298 - 344	+37.2 -28.6	+7.3 -7.1	+12.6 -7.5	+0.0 -3.0	+9.8 -8.5	± 4.3	± 1.6	+0.9 -0.9
344 - 396	+61.2 -39.2	+8.7 -8.3	+22.7 -11.7	+0.0 -3.0	+12.4 -9.4	± 4.2	± 2.8	+0.9 -0.9

systematic uncertainties (%) ($1.6 < |y^{\text{jet}}| < 2.1$)

p_T^{jet} [GeV/c]	jet energy scale	$\beta_{\text{DATA}}/\beta_{\text{MC}}$			resolution	unfolding	p_T^{jet} -spectra	$\delta_{\text{PT}}^{\text{MI}}$
54 - 62	+11.6 -10.3	+2.3 -2.1	—	—	+1.7 -1.6	± 3.2	± 1.0	+2.1 -2.0
62 - 72	+10.9 -10.1	+2.4 -2.4	—	—	+1.6 -1.7	± 3.3	± 0.8	+1.8 -1.8
72 - 83	+11.0 -10.3	+2.6 -2.6	—	—	+1.5 -1.7	± 3.4	± 0.6	+1.7 -1.7
83 - 96	+12.0 -11.1	+2.8 -2.9	—	—	+1.5 -1.8	± 3.5	± 0.4	+1.6 -1.6
96 - 110	+13.7 -12.5	+3.2 -3.2	—	—	+1.5 -1.8	± 3.6	± 0.3	+1.5 -1.5
110 - 127	+16.2 -14.4	+3.7 -3.5	—	—	+1.6 -1.9	± 3.7	± 0.2	+1.4 -1.4
127 - 146	+19.2 -16.9	+4.3 -4.0	—	—	+1.8 -2.0	± 3.7	± 0.1	+1.4 -1.4
146 - 169	+22.8 -19.8	+5.0 -4.6	—	—	+2.1 -2.1	± 3.8	± 0.2	+1.4 -1.3
169 - 195	+27.7 -23.0	+6.0 -5.4	+1.3 -0.9	—	+2.5 -2.3	± 3.8	± 0.5	+1.4 -1.3
195 - 224	+34.9 -26.7	+7.0 -6.4	+5.3 -5.6	—	+3.0 -2.7	± 3.8	± 1.1	+1.4 -1.3
224 - 259	+46.0 -32.4	+8.1 -8.0	+11.0 -11.1	—	+3.5 -3.3	± 3.8	± 2.1	+1.4 -1.3
259 - 298	+52.9 -39.2	+9.1 -8.3	+19.1 -11.7	—	+3.9 -3.0	± 3.8	± 2.7	+1.4 -1.3

$\frac{d^2\sigma}{dp_T^{\text{jet}} dy^{\text{jet}}} (y^{\text{jet}} < 0.1)$		
p_T^{jet} [GeV/c]	$\sigma \pm (\text{stat.}) \pm (\text{sys.})$ [nb/(GeV/c)]	C_{HAD} parton \rightarrow hadron
54 - 62	$(14.5 \pm 0.5^{+2.0}_{-1.9}) \times 10^0$	1.177 ± 0.124
62 - 72	$(6.68 \pm 0.08^{+0.85}_{-0.84}) \times 10^0$	1.144 ± 0.097
72 - 83	$(2.87 \pm 0.05^{+0.35}_{-0.34}) \times 10^0$	1.119 ± 0.077
83 - 96	$(1.24 \pm 0.02^{+0.14}_{-0.14}) \times 10^0$	1.098 ± 0.061
96 - 110	$(5.31 \pm 0.11^{+0.60}_{-0.61}) \times 10^{-1}$	1.083 ± 0.049
110 - 127	$(2.33 \pm 0.06^{+0.27}_{-0.26}) \times 10^{-1}$	1.070 ± 0.039
127 - 146	$(9.36 \pm 0.12^{+1.10}_{-1.08}) \times 10^{-2}$	1.060 ± 0.032
146 - 169	$(3.63 \pm 0.06^{+0.45}_{-0.43}) \times 10^{-2}$	1.052 ± 0.026
169 - 195	$(1.39 \pm 0.01^{+0.19}_{-0.18}) \times 10^{-2}$	1.046 ± 0.021
195 - 224	$(5.22 \pm 0.06^{+0.77}_{-0.72}) \times 10^{-3}$	1.041 ± 0.017
224 - 259	$(1.79 \pm 0.03^{+0.29}_{-0.27}) \times 10^{-3}$	1.037 ± 0.013
259 - 298	$(5.92 \pm 0.11^{+1.08}_{-1.00}) \times 10^{-4}$	1.034 ± 0.010
298 - 344	$(1.78 \pm 0.06^{+0.36}_{-0.33}) \times 10^{-4}$	1.032 ± 0.007
344 - 396	$(4.68 \pm 0.28^{+1.08}_{-0.94}) \times 10^{-5}$	1.030 ± 0.005
396 - 457	$(1.29 \pm 0.12^{+0.34}_{-0.29}) \times 10^{-5}$	1.028 ± 0.002
457 - 527	$(2.47 \pm 0.50^{+0.80}_{-0.68}) \times 10^{-6}$	1.027 ± 0.001
527 - 700	$(2.13 \pm 0.95^{+0.97}_{-0.75}) \times 10^{-7}$	1.026 ± 0.006

$\frac{d^2\sigma}{dp_T^{\text{jet}} dy^{\text{jet}}} (0.1 < y^{\text{jet}} < 0.7)$		
p_T^{jet} [GeV/c]	$\sigma \pm (\text{stat.}) \pm (\text{sys.})$ [nb/(GeV/c)]	C_{HAD} parton \rightarrow hadron
54 - 62	$(14.0 \pm 0.20^{+1.6}_{-1.6}) \times 10^0$	1.188 ± 0.140
62 - 72	$(6.14 \pm 0.12^{+0.66}_{-0.65}) \times 10^0$	1.156 ± 0.113
72 - 83	$(2.69 \pm 0.02^{+0.29}_{-0.27}) \times 10^0$	1.129 ± 0.091
83 - 96	$(1.14 \pm 0.01^{+0.12}_{-0.11}) \times 10^0$	1.108 ± 0.073
96 - 110	$(4.90 \pm 0.04^{+0.51}_{-0.48}) \times 10^{-1}$	1.090 ± 0.059
110 - 127	$(2.08 \pm 0.02^{+0.22}_{-0.21}) \times 10^{-1}$	1.076 ± 0.047
127 - 146	$(8.51 \pm 0.04^{+0.95}_{-0.89}) \times 10^{-2}$	1.065 ± 0.038
146 - 169	$(3.33 \pm 0.02^{+0.40}_{-0.37}) \times 10^{-2}$	1.055 ± 0.029
169 - 195	$(1.23 \pm 0.01^{+0.16}_{-0.15}) \times 10^{-2}$	1.047 ± 0.023
195 - 224	$(4.53 \pm 0.02^{+0.65}_{-0.61}) \times 10^{-3}$	1.041 ± 0.017
224 - 259	$(1.57 \pm 0.01^{+0.26}_{-0.24}) \times 10^{-3}$	1.036 ± 0.012
259 - 298	$(4.87 \pm 0.06^{+0.91}_{-0.83}) \times 10^{-4}$	1.031 ± 0.007
298 - 344	$(1.43 \pm 0.02^{+0.34}_{-0.27}) \times 10^{-4}$	1.028 ± 0.003
344 - 396	$(3.69 \pm 0.10^{+0.94}_{-0.80}) \times 10^{-5}$	1.025 ± 0.001
396 - 457	$(7.18 \pm 0.34^{+2.20}_{-1.80}) \times 10^{-6}$	1.023 ± 0.004
457 - 527	$(1.16 \pm 0.13^{+0.44}_{-0.35}) \times 10^{-6}$	1.021 ± 0.008
527 - 700	$(8.97 \pm 2.40^{+4.75}_{-3.64}) \times 10^{-8}$	1.018 ± 0.014

Table 4: Measured inclusive jet differential cross section as a function of p_T^{jet} for jets in the regions $|y^{\text{jet}}| < 0.1$ and $0.1 < |y^{\text{jet}}| < 0.7$. An additional 5.8% uncertainty on the luminosity is not included. The parton-to-hadron correction factors, $C_{\text{HAD}}(p_T^{\text{jet}}, y^{\text{jet}})$, are applied to the pQCD predictions.

$$\frac{d^2\sigma}{dp_T^{\text{jet}} dy^{\text{jet}}} \quad (0.7 < |y^{\text{jet}}| < 1.1)$$

p_T^{jet} [GeV/c]	$\sigma \pm (\text{stat.}) \pm (\text{sys.})$ [nb/(GeV/c)]	C_{HAD} parton \rightarrow hadron
54 - 62	$(12.3 \pm 0.2^{+1.5}_{-1.5}) \times 10^0$	1.169 ± 0.125
62 - 72	$(5.48 \pm 0.14^{+0.65}_{-0.65}) \times 10^0$	1.143 ± 0.103
72 - 83	$(2.40 \pm 0.02^{+0.28}_{-0.27}) \times 10^0$	1.120 ± 0.085
83 - 96	$(1.00 \pm 0.01^{+0.15}_{-0.11}) \times 10^0$	1.102 ± 0.070
96 - 110	$(4.15 \pm 0.05^{+0.48}_{-0.46}) \times 10^{-1}$	1.087 ± 0.057
110 - 127	$(1.73 \pm 0.03^{+0.21}_{-0.20}) \times 10^{-1}$	1.075 ± 0.047
127 - 146	$(6.83 \pm 0.05^{+0.87}_{-0.82}) \times 10^{-2}$	1.064 ± 0.038
146 - 169	$(2.52 \pm 0.03^{+0.35}_{-0.33}) \times 10^{-2}$	1.056 ± 0.031
169 - 195	$(8.95 \pm 0.06^{+1.36}_{-1.26}) \times 10^{-3}$	1.048 ± 0.024
195 - 224	$(3.04 \pm 0.02^{+0.51}_{-0.47}) \times 10^{-3}$	1.042 ± 0.019
224 - 259	$(9.52 \pm 0.11^{+1.82}_{-1.68}) \times 10^{-4}$	1.037 ± 0.014
259 - 298	$(2.53 \pm 0.05^{+0.56}_{-0.51}) \times 10^{-4}$	1.033 ± 0.009
298 - 344	$(6.18 \pm 0.17^{+1.64}_{-1.49}) \times 10^{-5}$	1.030 ± 0.005
344 - 396	$(1.11 \pm 0.07^{+0.36}_{-0.31}) \times 10^{-5}$	1.027 ± 0.001
396 - 457	$(1.53 \pm 0.20^{+0.65}_{-0.50}) \times 10^{-6}$	1.025 ± 0.003
457 - 527	$(2.17 \pm 0.72^{+1.25}_{-0.88}) \times 10^{-7}$	1.023 ± 0.007

$$\frac{d^2\sigma}{dp_T^{\text{jet}} dy^{\text{jet}}} \quad (1.1 < |y^{\text{jet}}| < 1.6)$$

p_T^{jet} [GeV/c]	$\sigma \pm (\text{stat.}) \pm (\text{sys.})$ [nb/(GeV/c)]	C_{HAD} parton \rightarrow hadron
54 - 62	$(11.0 \pm 0.3^{+1.4}_{-1.3}) \times 10^0$	1.160 ± 0.125
62 - 72	$(4.40 \pm 0.15^{+0.54}_{-0.53}) \times 10^0$	1.133 ± 0.101
72 - 83	$(1.82 \pm 0.06^{+0.22}_{-0.22}) \times 10^0$	1.111 ± 0.081
83 - 96	$(7.22 \pm 0.37^{+0.90}_{-0.90}) \times 10^{-1}$	1.094 ± 0.065
96 - 110	$(2.98 \pm 0.05^{+0.38}_{-0.38}) \times 10^{-1}$	1.080 ± 0.052
110 - 127	$(1.14 \pm 0.03^{+0.15}_{-0.15}) \times 10^{-1}$	1.068 ± 0.042
127 - 146	$(4.10 \pm 0.04^{+0.60}_{-0.60}) \times 10^{-2}$	1.059 ± 0.034
146 - 169	$(1.39 \pm 0.02^{+0.22}_{-0.23}) \times 10^{-2}$	1.051 ± 0.027
169 - 195	$(4.19 \pm 0.04^{+0.78}_{-0.76}) \times 10^{-3}$	1.045 ± 0.021
195 - 224	$(1.15 \pm 0.02^{+0.25}_{-0.24}) \times 10^{-3}$	1.040 ± 0.016
224 - 259	$(2.73 \pm 0.09^{+0.73}_{-0.64}) \times 10^{-4}$	1.036 ± 0.012
259 - 298	$(5.18 \pm 0.23^{+1.68}_{-1.39}) \times 10^{-5}$	1.033 ± 0.009
298 - 344	$(7.99 \pm 0.61^{+3.31}_{-2.56}) \times 10^{-6}$	1.030 ± 0.006
344 - 396	$(1.05 \pm 0.22^{+0.79}_{-0.43}) \times 10^{-6}$	1.028 ± 0.003

$$\frac{d^2\sigma}{dp_T^{\text{jet}} dy^{\text{jet}}} \quad (1.6 < |y^{\text{jet}}| < 2.1)$$

p_T^{jet} [GeV/c]	$\sigma \pm (\text{stat.}) \pm (\text{sys.})$ [nb/(GeV/c)]	C_{HAD} parton \rightarrow hadron
54 - 62	$(6.67 \pm 0.15^{+0.84}_{-0.75}) \times 10^0$	1.132 ± 0.104
62 - 72	$(2.68 \pm 0.02^{+0.32}_{-0.30}) \times 10^0$	1.116 ± 0.087
72 - 83	$(1.04 \pm 0.01^{+0.12}_{-0.12}) \times 10^0$	1.100 ± 0.072
83 - 96	$(3.77 \pm 0.04^{+0.49}_{-0.46}) \times 10^{-1}$	1.086 ± 0.058
96 - 110	$(1.32 \pm 0.02^{+0.19}_{-0.18}) \times 10^{-1}$	1.072 ± 0.045
110 - 127	$(4.18 \pm 0.04^{+0.72}_{-0.65}) \times 10^{-2}$	1.059 ± 0.033
127 - 146	$(1.21 \pm 0.02^{+0.24}_{-0.22}) \times 10^{-2}$	1.047 ± 0.022

$\frac{d^2\sigma}{dp_T^{\text{jet}} dy^{\text{jet}}} (0.1 < y^{\text{jet}} < 0.7) (D = 0.5)$		
p_T^{jet} [GeV/c]	$\sigma \pm (\text{stat.}) \pm (\text{sys.})$ [nb/(GeV/c)]	C_{HAD} parton \rightarrow hadron
54 - 62	$(10.5 \pm 0.2^{+1.2}_{-1.1}) \times 10^0$	1.089 ± 0.104
62 - 72	$(4.81 \pm 0.03^{+0.54}_{-0.50}) \times 10^0$	1.076 ± 0.086
72 - 83	$(2.09 \pm 0.01^{+0.23}_{-0.21}) \times 10^0$	1.064 ± 0.070
83 - 96	$(0.91 \pm 0.01^{+0.10}_{-0.09}) \times 10^0$	1.055 ± 0.057
96 - 110	$(3.95 \pm 0.04^{+0.42}_{-0.39}) \times 10^{-1}$	1.047 ± 0.047
110 - 127	$(1.71 \pm 0.02^{+0.18}_{-0.17}) \times 10^{-1}$	1.041 ± 0.037
127 - 146	$(0.71 \pm 0.01^{+0.08}_{-0.07}) \times 10^{-1}$	1.035 ± 0.029
146 - 169	$(2.76 \pm 0.02^{+0.32}_{-0.31}) \times 10^{-2}$	1.030 ± 0.023
169 - 195	$(1.04 \pm 0.01^{+0.14}_{-0.13}) \times 10^{-2}$	1.026 ± 0.017
195 - 224	$(3.87 \pm 0.02^{+0.57}_{-0.53}) \times 10^{-3}$	1.022 ± 0.012
224 - 259	$(1.34 \pm 0.01^{+0.23}_{-0.21}) \times 10^{-3}$	1.019 ± 0.008
259 - 298	$(4.26 \pm 0.04^{+0.83}_{-0.74}) \times 10^{-4}$	1.017 ± 0.005
298 - 344	$(1.22 \pm 0.02^{+0.28}_{-0.24}) \times 10^{-4}$	1.015 ± 0.002
344 - 396	$(3.16 \pm 0.09^{+0.82}_{-0.71}) \times 10^{-5}$	1.013 ± 0.001
396 - 457	$(6.30 \pm 0.32^{+1.96}_{-1.63}) \times 10^{-6}$	1.011 ± 0.002
457 - 527	$(1.01 \pm 0.12^{+0.40}_{-0.31}) \times 10^{-6}$	1.010 ± 0.003
527 - 700	$(0.83 \pm 0.23^{+0.44}_{-0.32}) \times 10^{-7}$	1.008 ± 0.005

$\frac{d^2\sigma}{dp_T^{\text{jet}} dy^{\text{jet}}} (0.1 < y^{\text{jet}} < 0.7) (D = 1.0)$		
p_T^{jet} [GeV/c]	$\sigma \pm (\text{stat.}) \pm (\text{sys.})$ [nb/(GeV/c)]	C_{HAD} parton \rightarrow hadron
54 - 62	$(20.0 \pm 0.2^{+2.6}_{-2.3}) \times 10^0$	1.372 ± 0.227
62 - 72	$(8.65 \pm 0.04^{+1.1}_{-1.0}) \times 10^0$	1.296 ± 0.171
72 - 83	$(3.59 \pm 0.02^{+0.42}_{-0.39}) \times 10^0$	1.236 ± 0.129
83 - 96	$(1.49 \pm 0.01^{+0.17}_{-0.16}) \times 10^0$	1.190 ± 0.098
96 - 110	$(6.27 \pm 0.05^{+0.70}_{-0.65}) \times 10^{-1}$	1.155 ± 0.075
110 - 127	$(2.63 \pm 0.03^{+0.29}_{-0.27}) \times 10^{-1}$	1.127 ± 0.057
127 - 146	$(1.05 \pm 0.01^{+0.12}_{-0.11}) \times 10^{-1}$	1.105 ± 0.044
146 - 169	$(4.04 \pm 0.03^{+0.48}_{-0.45}) \times 10^{-2}$	1.088 ± 0.034
169 - 195	$(1.48 \pm 0.01^{+0.19}_{-0.18}) \times 10^{-2}$	1.075 ± 0.026
195 - 224	$(5.41 \pm 0.02^{+0.77}_{-0.73}) \times 10^{-3}$	1.065 ± 0.019
224 - 259	$(1.86 \pm 0.01^{+0.30}_{-0.28}) \times 10^{-3}$	1.057 ± 0.013
259 - 298	$(5.77 \pm 0.04^{+1.05}_{-1.00}) \times 10^{-4}$	1.050 ± 0.008
298 - 344	$(1.70 \pm 0.02^{+0.36}_{-0.32}) \times 10^{-4}$	1.045 ± 0.003
344 - 396	$(4.26 \pm 0.10^{+1.05}_{-0.93}) \times 10^{-5}$	1.041 ± 0.003
396 - 457	$(8.17 \pm 0.36^{+2.49}_{-2.06}) \times 10^{-6}$	1.038 ± 0.009
457 - 527	$(1.39 \pm 0.14^{+0.55}_{-0.42}) \times 10^{-6}$	1.036 ± 0.015
527 - 700	$(1.19 \pm 0.27^{+0.60}_{-0.46}) \times 10^{-7}$	1.033 ± 0.027

Table 6: Measured inclusive jet differential cross section as a function of p_T^{jet} for jets in the region $0.1 < |y^{\text{jet}}| < 0.7$ using $D = 0.5$ and $D = 1.0$. An additional 5.8% uncertainty on the luminosity is not included. The parton-to-hadron correction factors, $C_{\text{HAD}}(p_T^{\text{jet}})$, are applied to the pQCD predictions.

systematic uncertainties (%) ($0.1 < y^{\text{jet}} < 0.7$) ($D = 0.5$)						
p_T^{jet}	jet energy scale	$\beta_{\text{DATA}}/\beta_{\text{MC}}$	resolution	unfolding	p_T^{jet} -spectra	$\delta_{\text{PT}}^{\text{MI}}$
54 - 62	+9.9 -9.2	—	+2.4 -2.3	± 5.4	± 0.6	+0.8 -0.8
62 - 72	+9.8 -9.0	—	+2.4 -2.2	± 4.8	± 0.6	+0.7 -0.7
72 - 83	+9.8 -8.9	—	+2.3 -2.2	± 4.3	± 0.6	+0.6 -0.7
83 - 96	+9.7 -8.9	—	+2.2 -2.1	± 3.8	± 0.6	+0.6 -0.6
96 - 110	+9.8 -9.0	—	+2.2 -2.1	± 3.4	± 0.6	+0.5 -0.5
110 - 127	+10.0 -9.4	—	+2.1 -2.0	± 3.1	± 0.6	+0.5 -0.5
127 - 146	+10.4 -9.9	—	+2.1 -2.0	± 2.8	± 0.6	+0.4 -0.4
146 - 169	+11.2 -10.8	—	+2.1 -2.0	± 2.5	± 0.5	+0.4 -0.4
169 - 195	+12.5 -11.9	—	+2.1 -2.1	± 2.3	± 0.4	+0.4 -0.4
195 - 224	+14.3 -13.3	—	+2.2 -2.2	± 2.1	± 0.3	+0.4 -0.3
224 - 259	+16.6 -15.0	—	+2.4 -2.4	± 1.9	± 0.2	+0.3 -0.3
259 - 298	+19.3 -17.0	—	+2.7 -2.7	± 1.8	± 0.1	+0.3 -0.3
298 - 344	+22.3 -19.4	—	+3.1 -3.2	± 1.6	± 0.1	+0.3 -0.3
344 - 396	+25.7 -22.1	—	+3.7 -3.8	± 1.5	± 0.2	+0.3 -0.3
396 - 457	+30.7 -25.5	—	+4.5 -4.6	± 1.4	± 0.5	+0.3 -0.3
457 - 527	+39.5 -29.7	—	+5.5 -5.6	± 1.3	± 1.3	+0.3 -0.2
527 - 700	+52.6 -37.7	—	+7.4 -7.3	± 1.2	± 4.2	+0.3 -0.2

systematic uncertainties (%) ($0.1 < y^{\text{jet}} < 0.7$) ($D = 1.0$)						
p_T^{jet}	jet energy scale	$\beta_{\text{DATA}}/\beta_{\text{MC}}$	resolution	unfolding	p_T^{jet} -spectra	$\delta_{\text{PT}}^{\text{MI}}$
54 - 62	+10.7 -9.4	—	+2.7 -2.7	± 5.6	± 0.4	+3.5 -2.9
62 - 72	+10.4 -9.3	—	+2.6 -2.5	± 4.9	± 0.4	+3.0 -2.6
72 - 83	+10.3 -9.2	—	+2.4 -2.4	± 4.2	± 0.4	+2.6 -2.4
83 - 96	+10.2 -9.2	—	+2.3 -2.3	± 3.7	± 0.4	+2.3 -2.2
96 - 110	+10.2 -9.3	—	+2.2 -2.2	± 3.2	± 0.4	+2.1 -2.0
110 - 127	+10.4 -9.6	—	+2.1 -2.1	± 2.8	± 0.4	+1.9 -1.8
127 - 146	+10.8 -10.1	—	+2.0 -2.0	± 2.5	± 0.4	+1.7 -1.7
146 - 169	+11.5 -10.8	—	+1.9 -1.9	± 2.1	± 0.4	+1.6 -1.6
169 - 195	+12.6 -11.8	—	+1.9 -2.0	± 1.9	± 0.4	+1.5 -1.4
195 - 224	+13.9 -13.1	—	+1.9 -2.0	± 1.6	± 0.3	+1.4 -1.3
224 - 259	+15.8 -14.7	—	+2.1 -2.2	± 1.4	± 0.3	+1.3 -1.3
259 - 298	+18.0 -16.6	—	+2.4 -2.5	± 1.3	± 0.2	+1.3 -1.2
298 - 344	+20.8 -18.8	—	+2.8 -2.9	± 1.1	± 0.2	+1.2 -1.1
344 - 396	+24.5 -21.4	—	+3.4 -3.6	± 1.0	± 0.2	+1.2 -1.1
396 - 457	+30.1 -24.7	—	+4.3 -4.4	± 0.8	± 0.5	+1.1 -1.0
457 - 527	+38.8 -29.5	— 34	+5.4 -5.4	± 0.7	± 1.1	+1.1 -1.0
527 - 700	+49.8 -37.6	—	+7.3 -7.2	± 0.6	± 3.4	+1.0 -0.9

Table 7: Systematic uncertainties (in percentage) on the measured inclusive jet differential cross section as a function of p_T^{jet} , for jets in the region $0.1 < |y^{\text{jet}}| < 0.7$ and using $D = 0.5$ and $D = 1.0$. An additional 5.8% uncertainty on the luminosity is not included.

A Correlations on systematic uncertainties

The correlations among systematic uncertainties in different p_T^{jet} bins and $|y^{\text{jet}}|$ regions are studied in detail.

- The uncertainty on the absolute jet energy scale is decomposed into different sources considered independent but fully correlated across p_T^{jet} bins and $|y^{\text{jet}}|$ regions. A $\pm 1.8\%$ uncertainty on the absolute energy scale, independent on p_T^{jet} , results from the sum in quadrature of four different contributions: a $\pm 0.5\%$ uncertainty from the calorimeter stability versus time, a $\pm 1.0\%$ uncertainty due to the modeling of the jet fragmentation, a $\pm 0.5\%$ uncertainty from the simulation of the electromagnetic calorimeter response, and a $\pm 1.3\%$ uncertainty from the simulation of the calorimeter response at the boundary between calorimeter towers. Other contributions to the absolute energy scale uncertainty come from the description of the calorimeter response to hadrons for different ranges in hadron momentum [37]. Table VIII shows the resulting relative contributions to the quoted systematic uncertainty on the measured cross sections related to the absolute jet energy scale uncertainty.
- The rest of the systematic uncertainties on the measured cross sections are also considered independent and fully correlated across p_T^{jet} bins and $|y^{\text{jet}}|$ regions, except those related to the $\beta_{\text{DATA}}/\beta_{\text{MC}}$ ratio, for which uncertainties in different $|y^{\text{jet}}|$ regions are uncorrelated.

A global χ^2 test is performed according to the formula

$$\chi^2 = \sum_{j=1}^{76} \frac{[\sigma_j^{\text{d}} - \sigma_j^{\text{th}}(\bar{s})]^2}{[\delta\sigma_j^{\text{d}}]^2 + [\delta\sigma_j^{\text{th}}(\bar{s})]^2} + \sum_{i=1}^{17} [s_i]^2, \quad (5)$$

where σ_j^{d} is the measured cross section for a given data point, σ_j^{th} is the corresponding prediction, and \bar{s} denotes the vector of standard deviations, s_i , for the different systematic uncertainties. The values for $\sigma_j^{\text{th}}(\bar{s})$ are obtained from the nominal pQCD NLO prediction, where \bar{s} includes the uncertainty on C_{HAD} but does not consider PDF uncertainties. The sums run over 76 data points and 17 independent sources of systematic uncertainty, and the χ^2 is minimized with respect to \bar{s} .

relative contribution (%) to the systematic uncertainty on $\frac{d^2\sigma}{dp_T^{\text{jet}} dy^{\text{jet}}}$ (absolute jet energy scale decomposition)				
p_T^{jet} bin	$\pm 1.8\%$ uncertainty	response to hadrons		
	on absolute jet energy scale	$p < 12$ GeV/c	$12 < p < 20$ GeV/c	$p > 20$ GeV/c
54 - 62	90.3	37.8	15.2	13.5
62 - 72	90.2	35.2	16.1	19.1
72 - 83	89.9	31.9	17.0	24.6
83 - 96	89.2	28.8	17.3	30.1
96 - 110	88.0	26.0	16.9	35.8
110 - 127	86.4	22.7	16.4	41.9
127 - 146	84.3	20.0	15.1	47.7
146 - 169	82.1	17.2	14.1	52.6
169 - 195	79.8	14.6	12.7	57.0
195 - 224	77.6	12.5	11.5	60.7
224 - 259	75.7	10.7	10.3	63.6
259 - 298	73.8	9.1	9.2	66.2
298 - 344	72.1	7.8	8.2	68.3
344 - 396	70.5	6.8	7.3	70.2
396 - 457	69.2	5.8	6.4	71.7
457 - 527	68.0	5.0	5.7	72.9
527 - 700	66.8	4.2	5.0	74.2

Table 8: Relative contributions (in percentage) to the quoted systematic uncertainty on the measured cross sections related to the absolute jet energy scale uncertainty. Sources are considered independent and fully correlated in p_T^{jet} and $|y^{\text{jet}}|$.